

1 **Deglaciation and postglacial evolution of the Cère Valley (Cantal, French Massif Central)**  
2 **based on geomorphological mapping, <sup>36</sup>Cl surface exposure dating and glacier**  
3 **modelling**

4 Arthur Ancrenaz<sup>1\*</sup>, Stéphane Pochat<sup>2</sup>, Vincent Rinterknecht<sup>3</sup>, Laura Rodríguez-Rodríguez<sup>4</sup>,  
5 Emmanuelle Defive<sup>1</sup>, Alexandre Poiraud<sup>1</sup>, Vincent Jomelli<sup>3</sup>, Irene Schimmelpfennig<sup>3</sup>, ASTER Team<sup>3\*\*</sup>

6 <sup>1</sup> Université Clermont Auvergne, CNRS, GEOLAB, F-63000 Clermont-Ferrand, France

7 <sup>2</sup> Laboratoire de Planétologie et Géosciences, LPG, UMR 6112, Nantes Université, CNRS, France.

8 <sup>3</sup> Aix Marseille Univ, CNRS, IRD, INRAE, CEREGE, BP 80, 13545 Aix-en-Provence Cedex 4, France

9 <sup>4</sup> Departamento de Geología, Universidad de Oviedo, c/ Jesús Arias de Velasco s/n, 33005 Oviedo, Spain

10

11 \*Corresponding author: [arthur.ancrenaz@doctorant.uca.fr](mailto:arthur.ancrenaz@doctorant.uca.fr)

12 \*\*ASTER Team: Georges Aumaître, D. Bourlès, K. Keddadouche.

13 **Keywords**

14 <sup>36</sup>Cl surface exposure dating; Glacial geomorphology; Paleoclimate; Late Pleistocene; Cantal

15 **Abstract**

16 The landform assemblage in the Cère Valley (Cantal, France) provides one of the most complete  
17 sequences for Late Pleistocene glacial fluctuations in the French Massif Central. However, the  
18 associated glacial chronology has been debated since the 1980's. This paper aims to improve the  
19 glacial chronology in the Cère Valley using <sup>36</sup>Cl surface exposure ages. Geomorphological results  
20 define two glacier stadials with reconstructed ELAs of  $1078 \pm 43$  and  $1152 \pm 34$  m above sea level.  
21 These results are comparable to those obtained in the Alps or the Pyrenees during the Last Glacial

22 Maximum (26 to 19.5 ka). However,  $^{36}\text{Cl}$  surface exposure ages are centred around the Younger Dryas  
23 (YD), between 13 to 11 ka ( $n = 4$ ). We suggest that these  $^{36}\text{Cl}$  ages are not related to a standstill during  
24 the YD but rather to the effects of the postglacial evolution of the Cère Valley. We investigate two  
25 geomorphological end member scenarios to explain the postponed exposure of sampled boulders: the  
26 Aurillac Lake scenario and the latter fluvial incision scenario. While the nature of the geomorphological  
27 events leading to the boulder exhumation is not fully resolved, we highlight a long phase of postglacial  
28 evolution in the Cère Valley.

## 29 **1 Introduction**

30 At present, the glacial history of the Cantal-Cézallier-Monts Dore (CCMD) in the French Massif Central  
31 is poorly known despite early observations of past glacial imprints (Boule, 1896, 1895; Glangeaud,  
32 1921; Julien and Laval, 1868; Rames, 1873) that led to numerous geomorphological studies (Boisse  
33 de Black, 1951; Goër de Hervé, 1972; Valadas, 1984; Van Dorsser, 1986, 1982; Veyret, 1978). This is  
34 especially true when it comes to the last glacial extents and timing for which large uncertainties remain  
35 (Defive et al., 2019; Etlicher and Goër de Hervé, 1988). The geomorphological reconstructions of the  
36 CCMD glacier system were based on a sequence of end moraines located in the main Cantal valleys  
37 (Cère, Authre, Jordanne, Alagnon, Rhue) and Monts Dore valleys (Dordogne, Tarentaine) (Boisse de  
38 Black, 1951; Goër de Hervé, 1972; Valadas, 1984; Veyret, 1978). Most of the glacial remnants were  
39 associated to the last glaciation and are used to define three glacial stadials. The oldest, inferred to  
40 correspond to the Local Last Glacial Maximum (LLGM), was defined by the outermost end moraines or  
41 till deposits. A younger glacier re-advance, locally named the Recurrence Event, was defined by end  
42 moraines located upstream of the LLGM deposits. The end of the Recurrence Event started with the  
43 lowland deglaciation, i.e. Artense plateau and lower parts of valleys and plateaus of the CCMD. A final  
44 cirque glacier stadial was represented by end moraines located in two main Cantal head valleys: the  
45 Impradine and Lagnon valleys (Valadas, 1984). In addition, isolated patches of till were interpreted as  
46 pre-LLGM deposits and were associated to Middle-Pleistocene glaciations, based on their location

47 downstream of the LLGM deposits and their more intense weathered aspect (Goër de Hervé, 1972;  
48 Van Dorsser, 1982; Veyret, 1978).

49 The existing chronologies of the deglaciation sequence were constrained by indirect  
50 paleoenvironmental data. The timing of the LLGM was correlated to the timing of the glacier maximum  
51 extent in the Alps (Veyret, 1978), which is attributed to the global Last Glacial Maximum (LGM) (27.5 to  
52 23.3 ka *sensu* Hughes and Gibbard, 2015). The timing of the last deglaciation in Cantalis constrained  
53 by a single radiocarbon age (Veyret-Mekdjian et al., 1978) obtained from the Lugarde kame terrace in  
54 the Santoire Valley at 900 m above sea level (a.s.l.) (north of Cantal; Fig. 1 for the location). This kame  
55 deposit includes a layer rich in organic matter dated from 17.1 to 15.7 ka cal BP (2 sigma radiocarbon  
56 age calibrated with the CLAM v.2.3.2 software and the “IntCal20” calibration curve; Blaauw, 2010;  
57 Reimer et al., 2020) that was buried by a till deposit associated with a glacier advance. In addition,  
58 indirect chronological boundaries for deglaciation steps were provided by a pollen stratigraphy  
59 established in the CCMD deglaciated slopes. The typical Oldest Dryas (18.5 to 15.3 ka *sensu* Degeai  
60 and Pastre, 2009) pollinic assemblage defined at the Lake Bouchet at 1250 m a.s.l (Fig. 1 for location)  
61 is *Artemisia* optimum with increasing *Juniperus* and *Betula* (Reille and Beaulieu, 1988). This  
62 assemblage was reported in the CCMD deglaciated slopes but not directly dated: (i) on the Artense  
63 plateau between ~400 to ~1000 m a.s.l. (Vergne, 1991), (ii) on the northern flank of the Cantal at the  
64 Taphanel site, 975 m a.s.l. (Ponel et al., 1991; Ponel and Russell Coope, 1990) and (iii) on the southern  
65 flank of the Cantal at the Peyre site, 1100 m a.s.l. (Miras et al., 2006) (Fig. 1 for the location). In the  
66 Aubrac Mounts, at the Roustières site (1195 m a.s.l.; Fig. 1), radiocarbon ages for this pollinic  
67 assemblage range between 17.7 and 15.0 ka cal BP (Gandouin et al., 2016; Ponel et al., 2016).  
68 According to these local paleoenvironmental data, two different relative chronologies for deglaciation  
69 steps in the CCMD are still debated (Veyret, 1978; Etlicher and Goër de Hervé, 1988):

70 - after Veyret (1978), the Recurrence Event buried the Lugarde kame terrace during the Oldest Dryas.  
71 CCMD lowlands were deglaciated at the end of the Oldest Dryas and the beginning of the Bølling-  
72 Allerød (15.3–12.8 ka *sensu* Degeai and Pastre, 2009). Finally, the timing of the cirque glacier stadial

73 was correlated with the Younger Dryas (YD) cold event, between 12.8–11.7 ka (*sensu* Degeai and  
74 Pastre, 2009).

75 - after Etlicher and Goër de Hervé (1988), the Recurrence Event was older than the Oldest Dryas. The  
76 till that buried the Lugarde kame terrace was associated with a minor glacier advance after the lowland  
77 deglaciation. This advance took place at the latest during the Oldest Dryas. The cirque glacier stadial  
78 was correlated with the Oldest Dryas or the Bølling-Allerød.

79 The latter relative chronology for the CCMD deglaciation steps (Etlicher and Goër de Hervé, 1988) is  
80 broadly supported by direct chronological constraints established in the neighbouring Aubrac Mounts  
81 by  $^{10}\text{Be}$  and  $^{26}\text{Al}$  exposure ages (Ancrenaz et al., 2022). In this area, glacial fluctuations from the LLGM  
82 to the last glacial advance were reported by geomorphological mapping and were dated between 27 to  
83 17 ka. The full deglaciation of the Aubrac was dated to ~17 ka, during the Oldest Dryas. These findings  
84 are comparable to findings obtained at a regional scale. For example, LGM glacier advances were  
85 identified in the Alps (Wirsig et al., 2016 and references therein), in the Pyrenees (Calvet et al., 2011;  
86 Reixach et al., 2021) and in the Iberian Peninsula (Domínguez-Villar et al., 2013). Glacier recessions  
87 started at ~19 ka in the Alps (Wirsig et al., 2016) or ~20 ka in the Pyrenees (Delmas et al., 2011) and  
88 the Oldest Dryas was recognized as a glacier recession period over the entire Mediterranean basin  
89 (Allard et al., 2021).

90 The aim of this study is to update the existing indirect and relative chronology for the CCMD glaciation  
91 by revising the morphostratigraphic framework in the Cère Valley (Cantal). We combined  $^{36}\text{Cl}$  surface  
92 exposure dating and former glacier geometry modelling to reconstruct paleo-ELA and associated  
93 climatic conditions during the last deglaciation. We chose the Cère Valley (Cantal) because the most  
94 complete sequence of glacier fluctuations in the CCMD, and by extension in the Massif Central, is  
95 preserved. Four main features were described: (i) the Tronquières moraine, a pre-LLGM glacial deposit,  
96 (ii) the Carnéjac terminal moraine and associated proglacial outwash that delimits the LLGM, (iii) the  
97 Polminhac recessional moraine delimiting the Recurrence Event and (iv) the Vic-sur-Cère end moraine  
98 delimiting a glacier standstill during the deglaciation.

## 99 2 Study area

100 The Cère Valley is one of the deepest (350 to 150 m) and longest (30 km) radial valley of the Cantal  
101 stratovolcano. As other Cantal valleys, the Cère Valley was formed by the combined action of fluvial  
102 and glacial erosion in favourable volcano-tectonic settings (Valadas, 1984). The upper part of the  
103 valley, from the Col de Font de Cère at 1290 m a.s.l. to the Pas de la Cère (~700 m a.s.l.), developed  
104 into Miocene trachyandesite along 15 km (Leibbrandt, 2011; Nehlig et al., 2001). The lower part of the  
105 Cère Valley, from the Pas de la Cère to the Aurillac basin was incised into Oligo-Miocene sediments  
106 and Pliocene volcanic breccias (i.e. debris avalanche or debris flow) (Arnaud et al., 2002). Valley  
107 slopes were affected by large landslides of various nature (mainly deep-seated gravitational slope  
108 deformation and rock fall) but of unknown age, and favoured by geological and topographic settings  
109 (Valadas, 1984; Van Dorsser, 1982, 1986).

110 During the LLGM, the Cantal glacier was a radially drained icefield or icecap ( $2.5 \times 10^3 \text{ km}^2$ ) with an  
111 accumulation zone centred over the north-western part of the Cantal (Goër de Hervé, 1972; Veyret,  
112 1978) (Fig. 1). Radial valleys, such as the Cère Valley, canalized glacier outlets from the central  
113 accumulation zone towards the margin. The orographic effect of the Cantal (west windward exposed  
114 slopes are much wetter than downwind exposed slopes) is responsible for the dissymmetric extent of  
115 valley glaciers (Veyret, 1978). The north-western Cantal valleys were occupied by longer glaciers, up  
116 to 30 km, and the eastern valleys were occupied by shorter glaciers, up to 20 km (Fig. 1). To the north,  
117 the Cantal, the Cézallier and the Monts Dore glaciers were coalescent forming the CCMD glacier  
118 system (Fig. 1). The Cère glacier extended from the Col de Fond de Cère to the Aurillac basin at ~600  
119 m. The particularity of the lower part of the Cère Valley is related to its flat bottom, with infilling of  
120 Pleistocene fluvio-glacial sediments (Van Dorsser, 1982; Veyret, 1978) reaching up to 10-20 m thick  
121 (Fig. 2).

## 122 **3 Methodology**

### 123 **3.1 Glacial features inventory**

124 Our geomorphological mapping aims at deciphering the distribution of late Pleistocene glacial landforms  
125 and sediments with special attention to ice-marginal landforms that indicate extents of former glaciers  
126 (Kleman and Borgström, 1996). Postglacial deposits, generated by slopes or fluvial processes, such as  
127 landslides, colluvial accumulation, alluvial fans or alluvial terraces were also mapped. The mapping was  
128 elaborated using (i) the inventory of glacial features from the literature (Boisse de Black, 1951; Valadas,  
129 1984; Van Dorsser, 1982; Veyret, 1978), (ii) aerial photography (25 cm resolution) and Digital Elevation  
130 Models (DEM; 1 m resolution from LIDAR) delivered by the Institut national de l'information  
131 géographique et forestière (IGN), and (iii) *in situ* (i.e. in the field) verification and description. Mapping  
132 was performed using a Geographical Information System (GIS) software (ArcGis).

### 133 **3.2 Surface exposure dating using <sup>36</sup>Cl**

#### 134 *3.2.1 Sampling strategy*

135 In the Cère Valley six moraine boulders were identified as suitable objects for surface exposure dating  
136 (Fig. 3). One was located on the Cavanhac plateau (sample CTL-04), three on the Carnéjac end-  
137 moraine (samples CTL-01, -02, -03) and two on the Polminhac end-moraine (samples CTL-20, -21)  
138 (Figs. 2 and 3). Samples for <sup>36</sup>Cl dating were collected in the field from top flat surfaces (up to 5 cm  
139 thick) of volcanic boulders (basalt and volcanic breccias) using a hammer and a chisel. Sampling was  
140 performed on moraine boulders with a broad base embedded in the glacial landform to minimise  
141 potential post-depositional disturbance. Sample locations and elevations were recorded using a hand-  
142 held GPS with elevations cross-checked with the DEM. Skyline measurements were taken using a  
143 compass-clinometer and topographic shielding factors were calculated using the skyline calculator  
144 within the CRONUS online calculator (Balco et al., 2008; [http://stoneage.ice-](http://stoneage.ice-d.org/math/skyline/skyline_in.html)  
145 [d.org/math/skyline/skyline\\_in.html](http://stoneage.ice-d.org/math/skyline/skyline_in.html); accessed on 14<sup>th</sup> September 2019). Sample information is reported  
146 in Table 1.

### 147 3.2.2 Sample preparation and age calculation

148 Samples were crushed and sieved to 250-500  $\mu\text{m}$  at CEREGE (Aix-en-Provence, France). Chlorine  
149 was extracted and purified from whole-rock samples to produce AgCl for accelerator mass spectrometry  
150 (AMS) analysis, following the procedure described by Schimmelpfennig et al. (2011). About 2 g of the  
151 bulk rock and 2 g of the chemically treated sample fractions were sent to SARM (Nancy, France) for  
152 chemical composition analyses (Tables 2 and 3).  $^{35}\text{Cl}/^{37}\text{Cl}$  and  $^{36}\text{Cl}/^{35}\text{Cl}$  ratios were measured by  
153 accelerator mass spectrometry at the 5 MV accelerator ASTER at CEREGE (Arnold et al., 2013). Use  
154 of an isotopically enriched carrier allows simultaneous determination of the  $^{36}\text{Cl}$  and the natural Cl  
155 concentrations of the dissolved samples. For normalisation of the  $^{36}\text{Cl}/^{35}\text{Cl}$  ratios, an in-house standard  
156 with a given  $^{36}\text{Cl}/^{35}\text{Cl}$  value of  $1.42 \pm 0.02 \times 10^{-12}$  was used (Merchel et al., 2011). Blank corrections  
157 were performed by subtracting the number of atoms of  $^{36}\text{Cl}$  and Cl in the blanks from those in the  
158 samples, respectively.

159 Cl-36 ages were calculated with the Excel® spreadsheet of Schimmelpfennig et al. (2009), using the  
160 time-invariant scaling method of Stone (2000) and employing the following  $^{36}\text{Cl}$  production rates,  
161 referenced to sea level and high latitude (SLHL):  $42.2 \pm 4.8$  atoms  $^{36}\text{Cl}$  (g Ca) $^{-1}$  yr $^{-1}$  for spallation of Ca  
162 (Schimmelpfennig et al., 2011),  $148.1 \pm 7.8$  atoms  $^{36}\text{Cl}$  (g K) $^{-1}$  yr $^{-1}$  for spallation of K (Schimmelpfennig  
163 et al., 2014),  $13.0 \pm 3.0$  atoms  $^{36}\text{Cl}$  (g Ti) $^{-1}$  yr $^{-1}$  for spallation of Ti (Fink et al., 2000),  $1.9 \pm 0.2$  atoms  $^{36}\text{Cl}$   
164 (g Fe) $^{-1}$  yr $^{-1}$  for spallation of Fe (Stone et al., 1996), and  $696 \pm 185$  neutrons (g air) $^{-1}$  yr $^{-1}$  for the production  
165 rate of epithermal neutrons from fast neutrons in the atmosphere at the land/atmosphere interface  
166 (Marrero et al., 2016a). A high-energy neutron attenuation length of  $160 \text{ g.cm}^{-2}$  was used.

167 As the values of several  $^{36}\text{Cl}$  production rates are still under discussion, most importantly the one for  
168 spallation of Ca (Schimmelpfennig et al., 2011, Marrero et al., 2016a), we also calculated the exposure  
169 ages using the calculator by Marrero et al. (2016b), which incorporates default production rates based  
170 on Marrero et al. (2016a) and the time-variant (“Lm”) rather than the time-invariant (“St”) scaling method  
171 used in the Excel® spreadsheet of Schimmelpfennig et al. (2009). Due to the variations in the sample  
172 compositions and thus target element concentrations (Table 3), this leads to ages being between 0.3

173 ka younger and 0.2 ka older than when applying the above-described methods. These differences do  
174 not affect our chronological reconstructions.

175 Typical value for erosion rates of crystalline rocks are comprised between 0.5 to 2.5 mm.ka<sup>-1</sup> in alpine  
176 environments (Balco, 2011) with a suggested value of 2 mm.ka<sup>-1</sup> at mid-latitude for homogenous rocks  
177 (André, 2002). Our sampled surfaces come from volcanic breccia boulders (CTL-02, -03, -04, -20)  
178 composed of diverse volcanic clasts embedded in a fissile matrix (Figs. 3B-3E). Erosion processes  
179 through physical or chemical weathering are expected to be efficient and conducive to higher erosion  
180 rates than for homogenous crystalline rocks. For example, in Gran Canaria, exposure ages and erosion  
181 rates obtained from basaltic clasts embedded in volcanic breccias were calculated using <sup>3</sup>He (Williams  
182 et al., 2005). Results ranged from 2.7 to 23.9 mm.ka<sup>-1</sup> for exposure ages between 25.6 to 226.2 ka. We  
183 applied three different erosion rates to our <sup>36</sup>Cl surface exposure ages: 0, 10 and 20 mm.ka<sup>-1</sup> to  
184 quantify effects of various erosion rates.

### 185 **3.3 Reconstruction of former glacier geometry, associated ELA and paleoclimatic** 186 **conditions**

#### 187 *3.3.1 3D glacier reconstruction and ELA estimation*

188 The geometry of the former Cère glacier was modelled in 3D using the GlaRe ArcToolBox for ArcGIS  
189 (Pellitero et al., 2016) for the three glacial stadials recognized in the field (section 3.2; Fig. 4). This  
190 model assumes a perfect plasticity behaviour for glacier ice and applies the numerical iterative solution  
191 to the Van der Veen's equation (Benn and Hulton, 2010). The basal shear stress value generally lies  
192 between 50 kPa and 150 kPa (Benn and Evans, 2010). The appropriate basal shear stress value was  
193 estimated to match the reconstructed ice thickness according to geomorphological markers on valley  
194 sides, i.e. lateral moraines. Ice-thickness profiles were reconstructed along 70 flowlines that were  
195 manually digitized along the main glacial valley trunk and its network tributaries. Glacier surface was  
196 interpolated using the *Topo to Raster* method to produce a 100 x 100 m cell-size resolution DEM of the  
197 former glacier surface topography. A valley-shape correction factor ( $f$ ) of 0.7 (average  $f$  value obtained  
198 from 79 valley cross sections) was applied to account for the valley morphology effect.



199 Paleo-Equilibrium Line Altitudes (Paleo-ELAs) were estimated using the ELA Calculation ToolBox for  
200 ArcGIS (Pellitero et al., 2015) and the Area-Altitude Balance Ratio (AABR) method. Different BR values  
201 were associated with different glacier/climate relationships and a range of 1.0 to 2.5 with 0.5 intervals  
202 was applied to consider the global BR value reported in Rea (2009). The mean with its standard  
203 deviation was then reported for each glacial stadial.

204 The Cère Valley topography was affected by landslides, especially deep-seated landslides. The  
205 topography of the paleo-glacier bed has an influence on the 3D glacier modelling and the ELA  
206 estimation (Pellitero et al., 2016, 2015). In absence of a robust chronology for the landslides, glacier  
207 modelling was run with both the post-landslide topography (i.e. the current topography) and the pre-  
208 landslide topography. The pre-landslide topography was reconstructed following the methodology  
209 exposed in Rodríguez-Rodríguez et al. (2018).

### 210 3.3.2 *Paleoclimatic reconstructions*

211 As no glaciers are currently present in the Massif Central, a direct comparison between the current ELA  
212 and former ELAs was impossible. In order to estimate the amplitude of ELA changes and to quantify  
213 the effect of oceanic influences that control the Cantal climate (Jubertie, 2006), the current theoretical  
214 ELA was assessed using current climatic conditions derived from 21 climatic stations located in western  
215 Cantal (Figs. 1 and 4A). Climatic conditions were extrapolated to higher altitude using a linear  
216 regression and plotted against the Ohmura equation (Fig. 4C) which provides a relationship between  
217 the Mean Summer Temperature (MST in °C) and the Mean Annual Precipitation (MAP in mm.yr<sup>-1</sup>) at  
218 the ELA (derived from an inventory of 70 glaciers in the world; Ohmura et al., 1992). By graphic read  
219 out, the intersection between the extrapolated current climatic conditions above Cantal summits and  
220 the Ohmura equation yielded a MST of  $7.6 \pm 0.3^\circ\text{C}$  and a MAP of  $3162 \pm 163 \text{ mm.yr}^{-1}$ . These climatic  
221 conditions were converted to elevation in m, using current altitudinal lapse rates of  $840 \text{ mm.yr}^{-1}.\text{km}^{-1}$   
222 and  $5.0 \text{ }^\circ\text{C.km}^{-1}$  (Fig. 4A). A similar lapse rate for MST has been reconstructed reflecting potential  
223 effects of dominant south-western influences in the Cère Valley (Valadas, 1984) to  $5.5^\circ\text{C.km}^{-1}$   
224 (Genevois et al., 2022). This yielded a current theoretical ELA at  $2759 \pm 28 \text{ m}$  (Fig. 4C). Higher

225 altitudinal lapse rate for MST (i.e.  $5.5^{\circ}\text{C}\cdot\text{km}^{-1}$ ) decreasing the current theoretical ELA to 2634 m a.s.l.  
226 Once the ELA was calculated for current climatic conditions and for former glacial stadials, MST values  
227 were calculated according to -90% to 0% change of MAP compared to present, using the Ohmura  
228 equation (Ohmura et al., 1992) and current climatic gradients. This assumption did not account for  
229 paleo-climatic gradients, prevailing during the LGM and the Last Glacial-to-Interglacial Transition (LGIT)  
230 in Europe (Heyman et al., 2013; Peyron et al., 1998).

231 Mean July Temperature (MJT) data reconstructed from chironomid assemblages of the Oldest Dryas  
232 and the YD at the Roustières sites were used to estimate theoretical MAP at the ELA (Figs. 1 and 4).  
233 These data indicate a MJT of 6 to 10 °C for the Oldest Dryas and 10 to 13 °C for the YD. These two  
234 periods are drier than today according to pollinic assemblages (Gandouin et al., 2016; Ponel et al.,  
235 2016). First, paleo-MJT were converted into MST using the current linear relationships (0.98 factor; Fig.  
236 4B). Then the summer cooling was estimated by comparing paleo-MST with current MST recorded by  
237 local climatic stations. This cooling was applied to the current climate in the Cère Valley to obtain  
238 theoretical MST during the period of interest. No correction for altitude was performed as the Roustières  
239 site altitude frame reconstructed ELAs for the Carnéjac and the Polminhac stadials. The Ohmura  
240 equation was used to calculate the associated MAP. As the Roustières elevation (1196 m a.s.l.)  
241 approximates the ELA reconstruction elevations for the Carnéjac and the Polminhac stadials, no  
242 elevation correction was performed on calculated MST and MAP.

## 243 **4 Results**

### 244 **4.1 Glacial geomorphology**

245 No significant glacial deposits were found in the upper part of the Cère Valley. Here, multiple head  
246 valleys with amphitheatre morphologies have developed in trachyandesitic rocks (Fig. 5A). These  
247 topographic settings were associated with limited ice accumulation, except for the Fond d'Alagnon  
248 glacial cirque in the Alagnon Valley which ice contributed to the Cère Valley glacier by a glacier  
249 transfluence towards the Fond de Cère pass (1290 m) (Fig. 5A). In contrast in the lower part of the Cère

250 Valley, large glacial landforms constituting a specific landform assemblage, such as moraines and  
251 proglacial outwash were found, particularly in the Aurillac basin (Fig. 6). Geomorphological observations  
252 allowed to partly reconstruct the deglaciation sequence despite disturbances caused by slope deposits  
253 (alluvial fans, colluvial accumulation and landslides) or fluvial processes (incision and aggradation of  
254 the valley floor) which may have masked, reworked or buried glacial landforms and associated deposits  
255 (Fig. 6).

256 All glacial and associated deposits identified in this work were located between the Tronquières moraine  
257 and the Pas de la Cère. The Tronquières moraine in the Aurillac basin (644 m a.s.l.; Figs. 2 and 6)  
258 materialise the maximal extent of the Cère glacier. According to geological cores (Fig. 2), these deposits  
259 are composed of diamicton 2 to 4m thick, interpreted as till of undetermined age. Three levels of terrace  
260 above the current Cère river: +10, +20, +30 m (Figs. 2 and 6) were identified on the eastern slope of  
261 the Tronquières moraine, at the Cère and the Jordanne rivers confluence. Around 5.5 km upstream of  
262 the Tronquières moraine, the Carnéjac end moraine (640 m a.s.l.) forms a transverse topographic ridge  
263 in the Cère Valley. This landform was associated to fluvio-glacial deposits forming a three-kilometre-  
264 long perched (+15 to +5 m) terrace above the current Cère river. Near the proximal Carnéjac end  
265 moraine slope, clayey sediments were reported (Figs. 2 and 6), interpreted as potential lacustrine  
266 deposits. The Polminhac end moraine (650 m a.s.l.), located 14 km upstream of the Tronquières  
267 moraine, is constituted of two individua, smooth and parallel ridges across the valley, Tronquières  
268 moraine (Fig. 2). An alluvial cone partly masked this end moraine. On the Cère Valley slopes, the La  
269 Pradelle lateral moraine (925 m a.s.l.) was identified (Figs. 6 and 7) and is associated to the Carnéjac  
270 stadial. In addition, isolated patches of till and isolated erratic boulders were found at the Vézac pass  
271 (665 m a.s.l.), at the Puy des Arbres pass (880 m a.s.l.) and at the Curebourse pass (1000 m a.s.l.).  
272 These glacial deposits attest of tansfluences of the Cère glacier towards secondary valleys (Fig. 6).  
273 The Vic-sur-Cère landform is interpreted as an alluvial fan in relation to a marked gully. These glacial  
274 landforms allow to define at least three glacier stadials. The Tronquières stadial for which the  
275 Tronquières moraine give a minimal extent. As no new observation were performed, the earlier  
276 assumption that associated these deposits to pre-LLGM glacial advance was not modified (Veyret,

277 1978). However, tills were identified between the Troquières moraine and the Carnéjac end moraine.  
278 Based on their fresh aspects, i. e. no weathering traces, these deposits are associated to the LLGM.  
279 The Carnéjac and the Polminhac stadials were associated to two glacier standstills during the  
280 deglaciation.

281 Between the Carnéjac end moraine and the Pas de la Cère, large landslides affected the valley slopes.  
282 The largest one was the Vixouze landslide in which till deposits filled longitudinal gullies that were  
283 subsequently moulded by subglacial erosion (Figs. 5C, 5E, 6 and 7). These observations suggest that  
284 the Vixouze landslide, and by extension other smaller landslides in the Cère Valley, occurred before  
285 the Carnéjac stadial.

## 286 4.2 Chronological results

287 All samples have  $^{36}\text{Cl}/^{35}\text{Cl}$  ratios in the range of  $8.9 - 14.8 \times 10^{-14}$  compared to two process blanks  
288 (BKCTL-01 & -02) with  $^{36}\text{Cl}/^{35}\text{Cl}$  ratios of  $2.32 \pm 0.6$  and  $0.12 \pm 0.04 \times 10^{-15}$ , respectively. Typical  
289 uncertainties for raw AMS data are 1.7 – 3.0% for  $^{35}\text{Cl}/^{37}\text{Cl}$  and 6.2 – 9.3% for  $^{36}\text{Cl}/^{35}\text{Cl}$ . Measurement  
290 results, calculated concentrations and surface exposure ages with their uncertainties are reported in  
291 Table 4.

292 For samples CTL-01 and CTL-03, the correction of surface exposure ages with a 10 and a 20  $\text{mm.k}^{-1}$   
293 erosion rates led to older ages (Table 4; Fig. 8. In these samples, Cl concentrations are low (~30 ppm;  
294 Table 4). All other samples (CTL-02, -04, -20 and -21) give younger exposure ages when applying 10  
295 and 20  $\text{mm.k}^{-1}$  of erosion rates (Fig. 8). This is counter-intuitive when correcting exposure ages for  
296 erosion but these samples have high Cl concentrations (between ~99 – 521 ppm; Table 4). This high  
297 Cl concentration induce higher  $^{36}\text{Cl}$  concentration in the subsurface than at the surface through low-  
298 energy-neutron capture by  $^{35}\text{Cl}$ .

299 Surface exposure ages corrected with a 10  $\text{mm.k}^{-1}$  erosion rate were assumed to best reflect boulders  
300 erosion since their exposure. The stratigraphically oldest erratic boulder (CTL-04) is isolated and  
301 located on the Cavanhac plateau and has an exposure age of  $13.5 \pm 3.9$  ka (Table 4). This sample was

302 taken from an erratic boulder associated with LLGM retreat, before the Carnéjac stadial (Figs. 3D, 6  
303 and 8). Three moraine boulders embedded in the Carnéjac end moraine were sampled (Table 4; Figs.  
304 3A-3C, 6 and 8). Sample CTL-01 was taken from a basaltic boulder characterized by fractures and  
305 jigsaw cracks (Fig. 6A). Samples CTL-02 and CTL-03 were taken from volcanic breccia boulders (Figs.  
306 3B and 3C). Surface exposure ages are clustered:  $12.6 \pm 1.2$  ka (CTL-01),  $12.0 \pm 2.2$  ka (CTL-02) and  
307  $12.2 \pm 1.1$  ka (CTL-03), whereby only CTL-02 was a Cl-rich sample. Two volcanic breccia boulders  
308 were sampled from the inner ridge of the Polminhac end moraine (Figs. 3E–3F, 6 and 8): CTL-20 (Cl-  
309 rich sample) yielded a maximum exposure age of  $12.1 \pm 2.6$  ka and CTL-21 an exposure age of  $0.9 \pm$   
310  $0.3$  ka. Due to its position near the Cère river (~40 m) and its small size (~0.2 m<sup>3</sup> above ground), the  
311 CTL-21 boulder is interpreted as an exhumed boulder associated with probable latter fluvial or  
312 anthropogenic end moraine erosion.

313 We note that <sup>36</sup>Cl surface exposure ages from two distant (~8 km) end moraines: the Carnéjac and the  
314 Polminhac moraines, are well clustered to ~12 ka (n = 4; Fig. 8). The interpretation of these ages is  
315 discussed in section 5.

### 316 **4.3 Glacier modelling**

317 We performed 3D reconstructions of the paleo- Cère glacier with the position of Carnéjac and  
318 Polminhac end-moraines. We extended glacier flow-line to the Font d'Alagnon glacial cirque to account  
319 the presence of glacier transfluence at this place (Fig. 5A). The elevation of the La Pradelle lateral  
320 moraine (Figs. 6 and 7B) indicate a paleo-ice thickness of 280 m, compatible with a basal shear stress  
321 of 25 kPa for the lower part of the Cere valley during the Carnéjac stadial. However, typical value of  
322 basal shear stress for valley glaciers were 50 – 150 kPa (Benn and Evans, 2010). Our low value for  
323 basal shear stress supports rapid basal sliding compatible with deformable sediments at the glacier  
324 bed. Such deformable sediments could be represented by Oligocene and Miocene uncemented clayey  
325 sediments or Late Pleistocene deposits, which composed the lower Cère valley floor (Fig. 2 and 6). For  
326 the uppermost half of the valley a basal shear stress value of 100 kPa was used. We note that  
327 topography of the glacier bed changed before and after the landslides. However, the two distinct

328 topographic configurations did not significantly affect the reconstructed paleo-glaciers and associated  
329 ELAs. An ELA of  $1078 \pm 43$  m a.s.l. for a pre-landslides topography was calculated, whereas an ELA  
330 of  $1091 \pm 43$  m a.s.l. for a post-landslides topography (Table 5). Because we found till, associated to  
331 the Carnéjac stadial, in transversal gullies of the Vixouze landslide (section 4.1): (i) we hypothesise that  
332 the age of majority of landslides in the Cère Valley are associated to pre-Carnéjac stadial periods and  
333 (ii) we chose the post-landslides topography to reconstruct the Carnéjac and the Polminhac stadials.  
334 The glacier modelling of the Polminhac stadial was processed using the same basal shear stress values  
335 as for the Carnéjac stadial. Only the main flowline was adjusted to match the respective end moraine.

336 During the Carnéjac stadial, only the Curebourse pass was reached by the paleo-glacier that potentially  
337 flowed over into the Goul valley (Figs. 6 and 7). The other two transfluences identified in the field were  
338 probably active during the LLGM or at times when more ice accumulated in the valley. Reconstructed  
339 ELAs for the Carnéjac stadial ( $1091 \pm 43$  m a.s.l.) and for the Polminhac stadial ( $1152 \pm 34$  m a.s.l.) are  
340 indistinguishable within uncertainties (Table 5). These ELA values were comparable to those  
341 reconstructed in Western Europe during the LGM (see Kuhlemann et al. 2008 for a synthesis).

342 Based on the MJT for the Oldest Dryas and the YD from the Roustières site, the associated MJT at the  
343 ELA were calculated and summarized in Table 5. Results indicate a 9.2 to 5.4 °C cooling for the Oldest  
344 Dryas with a +141 to +230% MAP at the ELA and a 5.4 to 2.6 °C cooling for the YD with a +230 to  
345 +305% MAP at the ELA compared to today (Table 5). During these two periods, the reconstructed MAP  
346 gives wetter climate than today, which is not consistent with local and regional paleoenvironmental data.  
347 This discrepancy is partially due to temperature being not cold enough to calculate the MAP at the  
348 ELAs. The source of this incompatibility is discussed in the following section.

## 349 **5 Interpretations and discussion**

### 350 **5.1 $^{36}\text{Cl}$ surface exposure ages interpretation: boulders exhumation related to a** 351 **postglacial event?**

352  $\text{Cl-36}$  surface exposure ages obtained in the Cère Valley range between 13 to 11 ka (Table 4) and are  
353 coeval with the YD ( $n = 3$  for the Carnéjac end moraine and  $n = 1$  for the Polminhac end moraine).  
354 Sample CTL-04 from the stratigraphically oldest boulder gives an older surface exposure age with a  
355 broad uncertainty (Table 4; Fig. 8). This exposure age could reflect a minimum age for the LLGM end  
356 but it is not further discussed here as it is a single dated erratic boulder.

357 The association of the Carnéjac or the Polminhac end moraines to the YD cold event is not plausible  
358 considering that:

- 359 - the existing relative and local chronologies for the CCMD glacier fluctuations (Veyret, 1978; Etlicher  
360 and Goër de Hervé, 1988). These early chronological hypotheses are supported by local  
361 paleoenvironmental data and surface exposure ages ( $^{10}\text{Be}$  and  $^{26}\text{Al}$ ) from the nearby Aubrac  
362 Mountains (Ancrenaz et al., 2022). Both paleoenvironmental and exposure ages support a  
363 deglaciation of the CCMD at the end of the Oldest Dryas (Fig. 8). During the YD, either only cirque  
364 glaciers occurred in the CCMD according to Veyret (1978) or the CCMD was fully deglaciated  
365 according to Etlicher and Goër de Hervé (1988).
- 366 - the ELAs and associated paleoclimatic conditions reconstructed for these two stadials in the Cère  
367 Valley (between  $1078 \pm 43$  to  $1152 \pm 34$  m; Table 5), are comparable to reconstructions from the  
368 Alps or the Pyrenees during the LGM or the early LGIT (Ivy-Ochs et al., 2008; Kuhlemann et al.,  
369 2008; Reixach et al., 2021).

370 Two explanations to this apparent time lag between the expected glacial chronology of the CCMD and  
371 the  $^{36}\text{Cl}$  surface exposure ages obtained in the Cère Valley (this study) are considered. First, existing  
372 relative glacial chronologies for the CCMD underestimate the intensity of glacial advances during the  
373 YD. This means that associated climatic conditions in the CCMD were colder than expected to sustain

374 these two major glacier stadials. Nevertheless, local paleoenvironmental data converge towards robust  
375 reconstructions of the YD in the CCMD (Juvigné et al., 1996; Miras et al., 2006; Miras and Guenet,  
376 2013; Ponel et al., 1991; Vergne, 1991), and are not consistent with our mapped glacier advances.

377 The second hypothesis relies on uncertainties regarding the geomorphological events leading to the  
378 exhumation of the sampled boulders. Indeed, boulders embedded in end moraines could record  
379 incomplete exposure histories ( Heyman et al., 2011) induced by geomorphological evolution of the end  
380 moraine. Two processes could lead to underestimated surface exposure ages: erosion of the sampled  
381 surfaces and incomplete exposure. Effects of erosion of the sampled surface were quantified by  
382 correcting surface exposure ages for various erosion rates and results show comparable ages (Table  
383 4; Fig. 8). Generally, incomplete exposure is regarded as the main limiting effect in the use of surface  
384 exposure ages (Heyman et al., 2011). Incomplete exposure encompasses effects of post-depositional  
385 burial or exhumation that led to underestimated surface exposure ages. For example, end moraine  
386 slopes destabilization after the deglaciation is considered as a main process leading to incomplete  
387 exposure of boulders, by boulder rolling, burial or latter exhumation through erosional processes (Allard  
388 et al., 2020; Heyman et al., 2011; Putkonen and Swanson, 2003; Tomkins et al., 2021; Zreda et al.,  
389 1994).

390 In the Cère Valley,  $^{36}\text{Cl}$  surface exposure ages obtained for the Carnéjac end moraine and the  
391 Polminhac end moraine were (i) interpreted as non-related glacial event and (ii) constrained between  
392 13 – 11 ka. We argue that these boulders experienced the same incomplete exposure history with a  
393 first phase of burial with complete shielding and then a simultaneous exhumation related to a unique  
394 and rapid geomorphological event concerning both the Carnéjac and the Polminhac end moraines. This  
395 geomorphological event took place after the deglaciation of the Cère Valley. This hypothesis is further  
396 developed in the following section.

## 397 **5.2 Geomorphological scenarios for the postglacial evolution of the Cère Valley**

398 Geomorphological observations concerning the postglacial evolution of the lower Cère Valley, between  
399 the Aurillac basin and the Pas de la Cère (Fig. 2 for location), are summarized here:



- 400 - geomorphological activities on valley slopes such as gullies incision, alluvial fans (Vic fan; Fig. 6),  
401 shallow landslides and colluvial accumulation,
- 402 - the valley floor is composed by up to 15 to 20 m of Pleistocene sediments, i.e. till, fluvio-glacial,  
403 fluvial or slope deposits, according to geological cores (Fig. 2).
- 404 - three terrace levels were identified in the Aurillac basin (+10, + 20 and + 30 m; Fig. 6).
- 405 - between the Carnéjac end moraine and the Pas de la Cère, two flat topographic levels on the valley  
406 floor are reported at 640 m: related to the Carnéjac end moraine and at 660 m: related to the  
407 Polminhac end moraine.
- 408 - finally, clayey deposits against the proximal slopes of the Carnéjac end moraines were identified  
409 and were interpreted as lacustrine clay from a moraine dammed proglacial lake by Veyret (1978).

410 The resulting landform-sediment assemblage is interpreted as a typical paraglacial landscape  
411 (Ballantyne, 2002). The Cère Valley filling is related to the water sediment continuity perturbation during  
412 its postglacial evolution, inducing intensive aggradation dynamics between the Carnéjac end moraine  
413 and the Pas de la Cère. Intense slope activities due to paraglacial conditions is enhanced by the overall  
414 lithologies of the Cère Valley tributaries (heterogenous volcanic breccias and trachytic rocks) favourable  
415 to glacial debuitressing, landsliding and fluvial erosion which support a perturbed water sediment  
416 continuity by enhanced sediment supply in the Cère Valley.

417 To explain the synchronous  $^{36}\text{Cl}$  surface exposure ages from the Carnéjac ( $n = 3$ ) and the Polminhac  
418 ( $n = 1$ ) end moraines separated by 8 km, we combined our (i) literature review, (ii) geological cores  
419 compilation and (iii) field work, to propose two complementary geomorphological scenarios: the Aurillac  
420 proglacial Lake and the postglacial Cère river fluvial incision. The two scenarios encompass potential  
421 evolutions of the Cère Valley leading to boulders burial. These scenarios rely on two major assumptions:  
422 the Carnéjac and the Polminhac stadials were coeval to glacier-favourable periods identified in the  
423 Aubrac Mounts between 25 to 17 ka and the Cère Valley deglaciation is coeval with the Aubrac  
424 Mountains deglaciation ~17 ka (Ancrenaz et al. 2022). In addition, potential effects of anthropogenic  
425 disturbances (agricultural activities and urbanization) were not accounted for in these scenarios.

#### 426 **The Aurillac proglacial Lake scenario**

427 The Tronquières moraine (644 m a.s.l.) is assumed to be LLGM deposits. During the Cère glacier retreat  
428 the Tronquières moraine could have dammed the valley, enclosing the Aurillac basin and producing a  
429 moraine-dammed proglacial lake: the Aurillac Lake (Fig. 9). The lake surface altitude reached between  
430 640 to 660 m a.s.l. (deepest part between ~50 and ~70 m in the Aurillac basin), was 18 km long at its  
431 maximum with a total surface ranged between 32 and 44 km<sup>2</sup>. The following Carnéjac and Polminhac  
432 stadials and their associated end moraines were deposited in a glacialacustrine environment (Fig. 9).  
433 The Aurillac Lake shielded, at least partially, boulders from the Carnéjac and the Polminhac end  
434 moraines from cosmic rays. At some point during deglaciation, the Tronquières moraine was breached  
435 by the Cère river, lowering the Aurillac proglacial Lake level and exposing the boulders. Carnéjac and  
436 Polminhac end moraines dammed the valley, producing secondary lakes that did not shielded end  
437 moraine crests and sampled boulders. As the Tronquières moraine was breached, fluvial terraces in  
438 the Aurillac basin are constructed while minor lakes subsisted in the Valley (Fig. 9). In this scenario,  
439 <sup>36</sup>Cl surface exposure ages from the Carnéjac and the Polminhac boulders (13 to 11 ka) are considered  
440 maximum ages for their exhumation and correspond to the timing of the Aurillac Lake drainage.

#### 441 **Postglacial fluvial incision scenario**

442 After the LLGM, the Cère Valley glacier retreated and the Carnéjac and the Polminhac stadials occurred  
443 during deglaciation. As no moraine-dammed lakes were present in the Aurillac basin, the Carnéjac and  
444 the Polminhac end moraines are deposited in ice-marginal environment. The construction of alluvial  
445 terraces in the Aurillac basin were coeval with the Cère Valley deglaciation. After the full deglaciation,  
446 the Carnéjac and the Polminhac end moraines produced moraine-dammed lakes associated with  
447 aggradation dynamics by lacustrine sedimentation in the valley floor. These dynamics are enhanced by  
448 intense slope activities. During this period of aggradation, end moraines were stable landforms and  
449 sampled boulders were buried and fully shielded by at minimum 4 m of till. The end of aggradation  
450 dynamics was associated to a change in the hydro-sedimentary dynamic, leading to the Cère river  
451 fluvial incision of end moraines. This erosional phase was responsible of the end moraines

452 destabilization leading to boulders exhumation. In this scenario,  $^{36}\text{Cl}$  surface exposure ages (13 to 11  
453 ka) reflected the end moraines stabilization after an intensive erosional phase associated to the end of  
454 postglacial aggradation dynamics.

455

456 Each of these two scenarios have limitations. For the Aurillac proglacial Lake scenario, the true age of  
457 the Tronquières moraine is still uncertain. However, the identification of fresh aspect tills in the Aurillac  
458 basin associated to the LLGM (this study) offset the pre-LLGM hypothesis from Veyret (1978). In  
459 addition, no lacustrine deposits were identified with certainty in the Aurillac basin. For the postglacial  
460 fluvial incision scenario, the well-preserved topography of the Carnéjac and the Polminhac end  
461 moraines was the main limitation, that indicated limited post-deposition erosion of these landforms.  
462 Furthermore, the important size of the sampled boulders (Fig. 3) favoured limited effects of postglacial  
463 exhumation through end moraine erosion (Heyman et al., 2016).

464 Despite these limitations, our two scenarios highlight the wide range of postglacial geomorphological  
465 events that could have affected the lower Cère valley morphology and then could have impacted the  
466  $^{36}\text{Cl}$  surface exposure ages of the boulders. The true postglacial evolution is probably a combination of  
467 the two geomorphological scenarios: moraine-dams breaching and consecutive fluvial incision. More  
468 precisely, it is highly probable that proglacial lakes between the Carnéjac and the Polminhac end  
469 moraines have subsisted for a longer time than the lake between Aurillac and Carnéjac (Fig. 9). This is  
470 suggested by the distinct evolution between the Aurillac basin, affected by a longer fluvial incision (three  
471 terrace levels for nearly 40 m of vertical incision), compared to the Carnéjac - Polminhac - Pas de la  
472 Cère area, where no fluvial terraces are observed (very limited incision of 10 m at the Carnéjac  
473 moraine).

474 The chronological signal recorded by our  $^{36}\text{Cl}$  ages, between 13 – 11 ka, occurred 5 ka after the  
475 deglaciation and records an abrupt change in the water sediment continuity in the Cère Valley. We  
476 interpret the chronological signal as an exhumation age of the sampled boulders, due to the end of  
477 aggradation dynamics and the beginning of fluvial incision that demarcated the end of the postglacial

478 evolution of the Cère Valley (Figs. 8 and 9). By comparison, in deglaciated valleys of the Alps, the  
479 postglacial valley filling duration was estimated to up to 7 ka (Brardinoni et al., 2018), that is consistent  
480 with our scenarios. The end of the valley filling is mainly controlled by the timing of the tributaries  
481 deglaciation, slope stabilization and climatic conditions (Brardinoni et al., 2018; Ravazzi et al., 2012). A  
482 combination of all three factors was expected to ended the postglacial adjustment of the Cère Valley  
483 (13 - 11 ka).

## 484 **6 Conclusions**

485 The Cère Valley was occupied by a glacier and sediment assemblages provided an opportunity to  
486 reconstruct glacial fluctuations in the CCMD. Revision of geomorphological arguments allows to identify  
487 three glacial stadials. The Tronquières moraine marks the last maximal extent of the glacier but it was  
488 not possible to identify if it was deposited by a pre-LLGM glacier advance or a LLGM glacier advance.  
489 As a working hypothesis we attributed the glacial deposits in the Aurillac basin to the LLGM. Two other  
490 glacier stadials: the Carnéjac and the Polminhac stadials are defined by end moraines that materialize  
491 two major glacial events. Large landslides in the Cère Valley pre-existed to at least, these two glacier  
492 stadials (presence of till in landslide counter slopes).  $^{36}\text{Cl}$  surface exposure ages from one erratic  
493 boulder, three boulders embedded in the Carnéjac end moraine and two boulders embedded in the  
494 Polminhac end moraine were obtained. Results are coeval to the Younger Dryas and range between  
495 13 to 11 ka. The ages are too young considering the hypothesised ages of these end moraines  
496 according to existing relative glacial chronologies in the CCMD and the direct glacial chronology from  
497 the nearby Aubrac Mountains. Moreover, 3D reconstructions and associated ELAs with prevailing  
498 climatic conditions (MST and MAP) calculated for the Carnéjac and the Polminhac stadials are  
499 comparable to those calculated for the LGM and the early LGIT in the Alps and the Pyrenees.

500 To explain the time lag between  $^{36}\text{Cl}$  surface exposure ages and expected end moraine ages, we  
501 investigated geomorphological scenarios that could have led to a latter exhumation of the sampled  
502 boulders. Using geomorphic observations, geological cores and  $^{36}\text{Cl}$  surface exposure ages, two  
503 scenarios were presented: the Aurillac proglacial Lake scenario and the postglacial fluvial incision

504 scenario. Each scenario explains plausible causes of boulders burial and then exhumation by one  
505 unique geomorphological event. The geomorphological scenario judged as the more plausible indicated  
506 that after the Cère Valley glaciation, between 25 to 17 ka, moraine-dammed lakes and intensive slope  
507 activities under paraglacial conditions conducted to the Cère Valley fill. During this period, the Carnjéac  
508 and the Polminhac end moraines were stable landforms with sampled boulders buried and shielding  
509 from cosmic rays. This postglacial evolution (>17 to ~12 ka) ended by the Cère river fluvial incision,  
510 eroding the base of the end moraines which lowered their surfaces and exposed sampled boulders  
511 (~12 ka). However, future geomorphological investigations in the CCMD are needed to validate and  
512 complete this scenario.

513 This work highlights that our  $^{36}\text{Cl}$  surface exposure ages are related to a major geomorphological event  
514 at the Cère Valley scale, during its postglacial evolution. Those geomorphological processes need to  
515 be fully understood and are complementary to direct chronologies and 3D glacier reconstructions to  
516 correctly reconstruct glacial fluctuations. In other formerly glaciated Cantal valleys, as the Alagnon  
517 Valley, the same landform assemblage is identified (flat valley floor filled by Pleistocene sediments).  
518 This highlights the potential complex postglacial evolution of several Cantal valleys that is still poorly  
519 known and for which this work provides a few first order hypotheses.

## 520 **7 Acknowledgments and funding**

521 The authors thank Mr Christophe Ribes and Mr Jean-Marie Lafon, inhabitants of Carnéjac, for giving  
522 us permission to access erratic boulders located on their properties.  $^{36}\text{Cl}$  analyses were performed at  
523 the ASTER AMS national facility (CEREGE, Aix-en-Provence), supported by the INSU/CNRS, by the  
524 ANR through the “Projets thématiques d’excellence” program for the “Equipements d’excellence”  
525 ASTER-CEREGE action, and by the Institut de Recherche pour le Développement (IRD). This project  
526 was co-funded by INSU-SYSTER and was partially funded by the Ice-Collapse project (The dynamics  
527 of ice sheet collapse in deglaciation periods) supported by the French Agence Nationale de la  
528 Recherche through grant ANR-18-CE01-0009.

529

## 530 8 Bibliographic references

- 531 Allard, J.L., Hughes, P.D., Woodward, J.C., 2021. Heinrich Stadial aridity forced Mediterranean-wide  
532 glacier retreat in the last cold stage. *Nat. Geosci.* 14, 197–205. [https://doi.org/10.1038/s41561-](https://doi.org/10.1038/s41561-021-00703-6)  
533 [021-00703-6](https://doi.org/10.1038/s41561-021-00703-6)
- 534 Allard, J.L., Hughes, P.D., Woodward, J.C., Fink, D., Simon, K., Wilcken, K.M., 2020. Late Pleistocene  
535 glaciers in Greece: A new  $^{36}\text{Cl}$  chronology. *Quaternary Science Reviews* 245, 106528.  
536 <https://doi.org/10.1016/j.quascirev.2020.106528>
- 537 Ancrenaz, A., Defive, E., Poiraud, A., 2020. Fluctuations glaciaires au Pléistocène supérieur dans les  
538 Monts d'Aubrac (Massif central, France): nouvelles données. *Géomorphologie: relief,*  
539 *processus, environnement* 26, 16. <https://doi.org/10.4000/geomorphologie.14516>
- 540 Ancrenaz, A., Braucher, R., Defive, E., Poiraud, A., Steiger, J., 2022. Last glacial fluctuations in the  
541 southwestern Massif Central, Aubrac (France): First direct chronology from cosmogenic  $^{10}\text{Be}$   
542 and  $^{26}\text{Al}$  exposure dating. *Quaternary Science Reviews* 285, 107500.  
543 <https://doi.org/10.1016/j.quascirev.2022.107500>
- 544 André, M.-F., 2002. Geomorphic evidence for recurrent cold-based ice conditions in Nordic uplands  
545 during the Quaternary glaciations (Aurivaara Plateau, North Sweden). *Norsk Geografisk*  
546 *Tidsskrift - Norwegian Journal of Geography* 56, 74–79.  
547 <https://doi.org/10.1080/002919502760056387>
- 548 Arnaud, N., Leyrit, H., Nehlig, P., Binet, F., Jamet, A., Vannier, W., 2002. Lahars on the north-western  
549 flank of the Cantal stratovolcan 11.
- 550 Arnold, M., Aumaître, G., Boursières, D.L., Keddadouche, K., Braucher, R., Finkel, R.C., Nottoli, E.,  
551 Benedetti, L., Merchel, S., 2013. The French accelerator mass spectrometry facility ASTER  
552 after 4 years: Status and recent developments on  $^{36}\text{Cl}$  and  $^{129}\text{I}$ . *Nuclear Instruments and*  
553 *Methods in Physics Research Section B: Beam Interactions with Materials and Atoms* 294,  
554 24–28. <https://doi.org/10.1016/j.nimb.2012.01.049>
- 555 Balco, G., 2011. Contributions and unrealized potential contributions of cosmogenic-nuclide exposure  
556 dating to glacier chronology, 1990–2010. *Quaternary Science Reviews* 30, 3–27.  
557 <https://doi.org/10.1016/j.quascirev.2010.11.003>
- 558 Balco, G., Stone, J.O., Lifton, N.A., Dunai, T.J., 2008. A complete and easily accessible means of  
559 calculating surface exposure ages or erosion rates from  $^{10}\text{Be}$  and  $^{26}\text{Al}$  measurements.  
560 *Quaternary Geochronology, Prospects for the New Frontiers of earth and Environmental*  
561 *Sciences* 3, 174–195. <https://doi.org/10.1016/j.quageo.2007.12.001>
- 562 Ballantyne, C.K., 2002. Paraglacial geomorphology. *Quaternary Science Reviews* 83.
- 563 Benn, D.I., Evans, D.J.A., 2010. *Glaciers and Glaciation, Second Edition.* ed. Hodder Education,  
564 London.
- 565 Benn, D.I., Hulton, N.R.J., 2010. An Excel™ spreadsheet program for reconstructing the surface  
566 profile of former mountain glaciers and ice caps. *Computers & Geosciences* 36, 605–610.  
567 <https://doi.org/10.1016/j.cageo.2009.09.016>
- 568 Blaauw, M., 2010. Methods and code for 'classical' age-modelling of radiocarbon sequences.  
569 *Quaternary Geochronology* 5, 512–518. <https://doi.org/10.1016/j.quageo.2010.01.002>

- 570 Boisse de Black, Y., 1951. Les glaciations de l'Auvergne : massif du Cantal, Cézallier, Monts-Dore,  
571 étude géographique et géologique. impr. Moderne, Aurillac.
- 572 Borchers, B., Marrero, S., Balco, G., Caffee, M., Goehring, B., Lifton, N., Nishiizumi, K., Phillips, F.,  
573 Schaefer, J., Stone, J., 2016. Geological calibration of spallation production rates in the  
574 CRONUS-Earth project. *Quaternary Geochronology* 31, 188–198.  
575 <https://doi.org/10.1016/j.quageo.2015.01.009>
- 576 Boule, M., 1896. La topographie glaciaire en Auvergne. *Annales de Géographie* 5, 277–296.  
577 <https://doi.org/10.3406/geo.1896.6883>
- 578 Boule, M., 1895. Les glaciers pliocènes et quaternaires de l'Auvergne. *Comptes rendus*  
579 *hebdomadaires des séances de l'Académie des Sciences* 121, 837–839.
- 580 Brardinoni, F., Picotti, V., Maraio, S., Bruno, P.P., Cucato, M., Morelli, C., Mair, V., 2018. Postglacial  
581 evolution of a formerly glaciated valley: Reconstructing sediment supply, fan building, and  
582 confluence effects at the millennial time scale. *GSA Bulletin* 130, 1457–1473.  
583 <https://doi.org/10.1130/B31924.1>
- 584 Calvet, M., Delmas, M., Gunnell, Y., Braucher, R., Bourlès, D., 2011. Recent Advances in Research  
585 on Quaternary Glaciations in the Pyrenees, in: *Developments in Quaternary Sciences*.  
586 Elsevier, pp. 127–139. <https://doi.org/10.1016/B978-0-444-53447-7.00011-8>
- 587 Degeai, J.-P., Pastre, J.-F., 2009. Impacts environnementaux sur l'érosion des sols au Pléistocène  
588 supérieur et à L'holocène dans le cratère de maar du lac du Bouchet (Massif central, France).  
589 *quaternaire* 149–159. <https://doi.org/10.4000/quaternaire.5101>
- 590 Defive, E., Raynal, J.P., Ancrenaz, A., Poiraud, A., 2019. L'englacement quaternaire du Massif central,  
591 in: *Histoire de la découverte géologique du Massif central français, Mémoire. Société d'Histoire*  
592 *Naturelle d'Auvergne*, p. 267.
- 593 Delmas, M., Calvet, M., Gunnell, Y., Braucher, R., Bourlès, D., 2011. Palaeogeography and  $^{10}\text{Be}$   
594 exposure-age chronology of Middle and Late Pleistocene glacier systems in the northern  
595 Pyrenees: Implications for reconstructing regional palaeoclimates. *Palaeogeography,*  
596 *Palaeoclimatology, Palaeoecology* 305, 109–122.  
597 <https://doi.org/10.1016/j.palaeo.2011.02.025>
- 598 Ehlers, J., Gibbard, P.L., Hughes, P.D., 2011. *Quaternary Glaciations - Extent and Chronology,*  
599 Elsevier. ed, *Developments in Quaternary Science*.
- 600 Etlicher, B., Goër de Hervé, A. (de), 1988. La déglaciation würmienne dans le Massif Central français,  
601 le point des travaux récents / The Würmian déglaciation in the French Massif-Central, review  
602 of recent works., *Bulletin de l'Association française pour l'étude du quaternaire* 25, 103–110.  
603 <https://doi.org/10.3406/quate.1988.1871>
- 604 Fink, D., Vogt, S., Hotchkis, M., 2000. Cross-sections for  $^{36}\text{Cl}$  from Ti at  $E_p=35\text{--}150\text{ MeV}$ :  
605 Applications to in-situ exposure dating. *Nuclear Instruments and Methods in Physics Research*  
606 *Section B: Beam Interactions with Materials and Atoms* 172, 861–866.  
607 [https://doi.org/10.1016/S0168-583X\(00\)00200-7](https://doi.org/10.1016/S0168-583X(00)00200-7)
- 608 Gandouin, E., Rioual, P., Pailles, C., Brooks, S.J., Ponel, P., Guiter, F., Djamali, M., Andrieu-Ponel,  
609 V., Birks, H.J.B., Leydet, M., Belkacem, D., Haas, J.N., Van der Putten, N., de Beaulieu, J.L.,  
610 2016. Environmental and climate reconstruction of the late-glacial-Holocene transition from a  
611 lake sediment sequence in Aubrac, French Massif Central: Chironomid and diatom evidence.

- 612 Palaeogeography, Palaeoclimatology, Palaeoecology 461, 292–309.  
613 <https://doi.org/10.1016/j.palaeo.2016.08.039>
- 614 Genevois, V., Martin, C., Morel, J.-M., Poiraud, A., Suc, O., Laveuf, C., Vautier, A., Decugis, E.,  
615 Marcou, P., Foret, M., Rahimian, V., 2022. Référenciel Régional Pédologique du Cantal, étude  
616 n°30150.
- 617 Glangeaud, P., 1921. Essai de synthèse sur les anciens glaciers du Massif central. Compte rendu  
618 sommaire Société Géologique de France 119.
- 619 Goër de Hervé, A. (de), 1972. La Planèze de Saint-Flour : structure et géomorphologie glaciaire. Univ.  
620 Clermont II.
- 621 Heyman, B.M., Heyman, J., Fickert, T., Harbor, J.M., 2013. Paleo-climate of the central European  
622 uplands during the last glacial maximum based on glacier mass-balance modeling. *Quat. res.*  
623 79, 49–54. <https://doi.org/10.1016/j.yqres.2012.09.005>
- 624 Heyman, J., Applegate, P.J., Blomdin, R., Gribenski, N., Harbor, J.M., Stroeven, A.P., 2016. Boulder  
625 height – exposure age relationships from a global glacial <sup>10</sup>Be compilation. *Quaternary*  
626 *Geochronology* 34, 1–11. <https://doi.org/10.1016/j.quageo.2016.03.002>
- 627 Heyman, J., Stroeven, A.P., Harbor, J.M., Caffee, M.W., 2011. Too young or too old: Evaluating  
628 cosmogenic exposure dating based on an analysis of compiled boulder exposure ages. *Earth*  
629 *and Planetary Science Letters* 302, 71–80. <https://doi.org/10.1016/j.epsl.2010.11.040>
- 630 Hughes, P.D., Gibbard, P.L., 2015. A stratigraphical basis for the Last Glacial Maximum (LGM).  
631 *Quaternary International* 383, 174–185. <https://doi.org/10.1016/j.quaint.2014.06.006>
- 632 Ivy-Ochs, S., Kerschner, H., Reuther, A., Preusser, F., Heine, K., Maisch, M., Kubik, P.W., Schlüchter,  
633 C., 2008. Chronology of the last glacial cycle in the European Alps. *J. Quaternary Sci.* 23, 559–  
634 573. <https://doi.org/10.1002/jqs.1202>
- 635 Jubertie, F., 2006. Les excès climatiques dans le Massif central français. L'impact des temps forts  
636 pluviométriques et anémométriques en Auvergne. Université Blaise Pascal - Clermont Ferrand  
637 II.
- 638 Julien, A., Laval, E., 1868. Sur l'existence d'anciens glaciers dans le Puy-de-Dôme et le Cantal, et sur  
639 l'origine véritable des conglomérats ponceux de la colline de Perrier. *Comptes rendus*  
640 *hebdomadaires des séances de l'Académie des Sciences* 67, 1356–1357.
- 641 Juvigné, E., Bastin, B., Delibrias, G., Evin, J., Gewalt, M., Gilot, E., Streef, M., 1996. A comprehensive  
642 pollen- and tephra-based chronostratigraphic model for the Late Glacial and Holocene period  
643 in the French Massif Central. *Quaternary International* 34–36, 113–120.  
644 [https://doi.org/10.1016/1040-6182\(95\)00075-5](https://doi.org/10.1016/1040-6182(95)00075-5)
- 645 Kleman, J., Borgström, I., 1996. RECONSTRUCTION OF PALAEO-ICE SHEETS: THE USE OF  
646 GEOMORPHOLOGICAL DATA. *Earth Surface Processes and Landforms* 21, 893–909.  
647 [https://doi.org/10.1002/\(SICI\)1096-9837\(199610\)21:10<893::AID-ESP620>3.0.CO;2-U](https://doi.org/10.1002/(SICI)1096-9837(199610)21:10<893::AID-ESP620>3.0.CO;2-U)
- 648 Kuhlemann, J., Rohling, E.J., Krumrei, I., Kubik, P., Ivy-Ochs, S., Kucera, M., 2008. Regional  
649 Synthesis of Mediterranean Atmospheric Circulation During the Last Glacial Maximum.  
650 *Science* 321, 1338–1340. <https://doi.org/10.1126/science.1157638>
- 651 Leibbrandt, S., 2011. Reconstitution de l'évolution morpho-structurale et de la dynamique éruptive du  
652 massif du Cantal: relation avec la distribution spatio-temporelle du volcanisme du Massif  
653 Central (France). Univ. Paris Sud 2.



- 654 Marrero, S.M., Phillips, F.M., Borchers, B., Lifton, N., Aumer, R., Balco, G., 2016a. Cosmogenic  
655 nuclide systematics and the CRONUScalc program. *Quaternary Geochronology* 31, 160–187.  
656 <https://doi.org/10.1016/j.quageo.2015.09.005>
- 657 Marrero, S.M., Phillips, F.M., Caffee, M.W., Gosse, J.C., 2016b. CRONUS-Earth cosmogenic <sup>36</sup>Cl  
658 calibration. *Quaternary Geochronology* 31, 199–219.  
659 <https://doi.org/10.1016/j.quageo.2015.10.002>
- 660 Merchel, S., Bremser, W., Alfimov, V., Arnold, M., Aumaître, G., Benedetti, L., Bourlès, D.L., Caffee,  
661 M., Fifield, L.K., Finkel, R.C., Freeman, S.P.H.T., Martschini, M., Matsushi, Y., Rood, D.H.,  
662 Sasa, K., Steier, P., Takahashi, T., Tamari, M., Tims, S.G., Tosaki, Y., Wilcken, K.M., Xu, S.,  
663 2011. Ultra-trace analysis of <sup>36</sup>Cl by accelerator mass spectrometry: an interlaboratory study.  
664 *Anal Bioanal Chem* 400, 3125–3132. <https://doi.org/10.1007/s00216-011-4979-2>
- 665 Miras, Y., Guenet, P., 2013. Une histoire plurimillénaire des paysages du Cézallier et ses liens avec  
666 les activités agrosylvo- pastorales depuis le Néolithique à partir de l'analyse pollinique de la  
667 tourbière de La Borie (1170 m, Saint-Saturnin, Cantal) 17.
- 668 Miras, Y., Surmely, F., Guenet, P., Vannièrre, B., Walter-Simonnet, A.-V., 2006. Dynamiques  
669 d'occupation et histoire de l'environnement d'un terroir de moyenne montagne : la tourbière de  
670 Peyre (Lacapelle-Barrès, Cantal, Massif central) et ses alentours. *Premiers résultats* 27.
- 671 Murton, J.B., Ballantyne, C.K., 2017. Chapter 5 Periglacial and permafrost ground models for Great  
672 Britain. *EGSP* 28, 501–597. <https://doi.org/10.1144/EGSP28.5>
- 673 Nehlig, P., Leyrit, H., Dardon, A., Freour, G., de Goër, A., Huguet, D., Thieblemont, D., 2001.  
674 Constructions et destructions du stratovolcan du Cantal. *Bulletin de la Société Géologique de*  
675 *France* 172, 295–308.
- 676 Ohmura, A., Kasser, P., Funk, M., 1992. Climate at the equilibrium line of glaciers. *Journal of*  
677 *Glaciology* 38, 397–411.
- 678 Pellitero, R., Rea, B.R., Spagnolo, M., Bakke, J., Hughes, P., Ivy-Ochs, S., Lukas, S., Ribolini, A.,  
679 2015. A GIS tool for automatic calculation of glacier equilibrium-line altitudes. *Computers &*  
680 *Geosciences* 82, 55–62. <https://doi.org/10.1016/j.cageo.2015.05.005>
- 681 Pellitero, R., Rea, B.R., Spagnolo, M., Bakke, J., Ivy-Ochs, S., Frew, C.R., Hughes, P., Ribolini, A.,  
682 Lukas, S., Renssen, H., 2016. GlaRe, a GIS tool to reconstruct the 3D surface of  
683 palaeoglaciers. *Computers & Geosciences* 94, 77–85.  
684 <https://doi.org/10.1016/j.cageo.2016.06.008>
- 685 Peyron, O., Guiot, J., Cheddadi, R., Tarasov, P., Reille, M., de Beaulieu, J.-L., Bottema, S., Andrieu,  
686 V., 1998. Climatic Reconstruction in Europe for 18,000 YR B.P. from Pollen Data. *Quaternary*  
687 *Research* 49, 183–196. <https://doi.org/10.1006/qres.1997.1961>
- 688 Ponel, P., Etlicher, B., De Beaulieu, J.L., Debard, E., Thinon, M., Vasari, A., Petiot, R., 1991. La fin  
689 de la dernière glaciation dans le Cantal (France): la tourbière de La Taphanel et son  
690 environnement. *Quaternaire* 2, 147–163. <https://doi.org/10.3406/quate.1991.1964>
- 691 Ponel, P., Guiter, F., Gandouin, E., Pailles, C., Rioual, P., Djamali, M., Andrieu-Ponel, V., Leydet, M.,  
692 Van der Putten, N., de Beaulieu, J.-L., 2016. Novel insights from coleopteran and pollen  
693 evidence into the Lateglacial/Holocene transition in Aubrac, French Massif Central.  
694 *Palaeogeography, Palaeoclimatology, Palaeoecology* 463, 83–102.  
695 <https://doi.org/10.1016/j.palaeo.2016.09.020>

- 696 Ponel, P., Russell Coope, G., 1990. Lateglacial and Early Flandrian Coleoptera from La Taphanel,  
697 Massif Central, France: Climatic and Ecological Implications. *Journal of Quaternary Science*  
698 5, 235–249. <https://doi.org/10.1002/jqs.3390050306>
- 699 Putkonen, J., Swanson, T., 2003. Accuracy of cosmogenic ages for moraines. *Quaternary Research*  
700 59, 255–261. [https://doi.org/10.1016/S0033-5894\(03\)00006-1](https://doi.org/10.1016/S0033-5894(03)00006-1)
- 701 Rames, J.-B., 1873. Géogénie du Cantal avec une étude historique et critique sur les progrès des la  
702 géologie dans ce département. 116.
- 703 Ravazzi, C., Badino, F., Marsetti, D., Patera, G., Reimer, P.J., 2012. Glacial to paraglacial history and  
704 forest recovery in the Oglia glacier system (Italian Alps) between 26 and 15 ka cal BP.  
705 *Quaternary Science Reviews* 58, 146–161. <https://doi.org/10.1016/j.quascirev.2012.10.017>
- 706 Rea, B.R., 2009. Defining modern day Area-Altitude Balance Ratios (AABRs) and their use in glacier-  
707 climate reconstructions. *Quaternary Science Reviews* 28, 237–248.  
708 <https://doi.org/10.1016/j.quascirev.2008.10.011>
- 709 Reille, M., Beaulieu, J.-L. (de), 1988. History of the Würm and Holocene vegetation in western Velay  
710 (Massif Central, France): a comparison of pollen analysis from three corings at Lac du  
711 Bouchet. *Review of Palaeobotany and Palynology* 54, 233–248
- 712 Reimer, P.J., Austin, W.E.N., Bard, E., Bayliss, A., Blackwell, P.G., Bronk Ramsey, C., Butzin, M.,  
713 Cheng, H., Edwards, R.L., Friedrich, M., Grootes, P.M., Guilderson, T.P., Hajdas, I., Heaton,  
714 T.J., Hogg, A.G., Hughen, K.A., Kromer, B., Manning, S.W., Muscheler, R., Palmer, J.G.,  
715 Pearson, C., van der Plicht, J., Reimer, R.W., Richards, D.A., Scott, E.M., Southon, J.R.,  
716 Turney, C.S.M., Wacker, L., Adolphi, F., Büntgen, U., Capano, M., Fahrni, S.M., Fogtmann-  
717 Schulz, A., Friedrich, R., Köhler, P., Kudsk, S., Miyake, F., Olsen, J., Reinig, F., Sakamoto,  
718 M., Sookdeo, A., Talamo, S., 2020. The IntCal20 Northern Hemisphere Radiocarbon Age  
719 Calibration Curve (0–55 cal kBP). *Radiocarbon* 62, 725–757.  
720 <https://doi.org/10.1017/RDC.2020.41>
- 721 Reixach, T., Delmas, M., Braucher, R., Gunnell, Y., Mahé, C., Calvet, M., 2021. Climatic conditions  
722 between 19 and 12 ka in the eastern Pyrenees, and wider implications for atmospheric  
723 circulation patterns in Europe. *Quaternary Science Reviews* 260, 106923.  
724 <https://doi.org/10.1016/j.quascirev.2021.106923>
- 725 Rodríguez-Rodríguez, L., González-Lemos, S., Ballesteros, D., Valenzuela, P., Domínguez-Cuesta,  
726 M.J., Llana-Fúnez, S., Jiménez-Sánchez, M., 2018. Timing of paraglacial rock-slope failures  
727 and denudation signatures in the Cantabrian Mountains (North Iberian Peninsula). *Land*  
728 *Degrad Dev* 29, 3159–3173. <https://doi.org/10.1002/ldr.3012>
- 729 Schimmelpfennig, I., Benedetti, L., Finkel, R., Pik, R., Blard, P.-H., Bourlès, D., Burnard, P., Williams,  
730 A., 2009. Sources of in-situ  $^{36}\text{Cl}$  in basaltic rocks. Implications for calibration of production  
731 rates. *Quaternary Geochronology* 4, 441–461. <https://doi.org/10.1016/j.quageo.2009.06.003>
- 732 Schimmelpfennig, I., Benedetti, L., Garreta, V., Pik, R., Blard, P.-H., Burnard, P., Bourlès, D., Finkel,  
733 R., Ammon, K., Dunai, T., 2011. Calibration of cosmogenic  $^{36}\text{Cl}$  production rates from Ca and  
734 K spallation in lava flows from Mt. Etna (38°N, Italy) and Payun Matru (36°S, Argentina).  
735 *Geochimica et Cosmochimica Acta* 75, 2611–2632. <https://doi.org/10.1016/j.gca.2011.02.013>
- 736 Schimmelpfennig, I., Schaefer, J.M., Putnam, A.E., Koffman, T., Benedetti, L., Ivy-Ochs, S., Team,  
737 A., Schlüchter, C., 2014.  $^{36}\text{Cl}$  production rate from K-spallation in the European Alps  
738 (Chironico landslide, Switzerland):  $^{36}\text{Cl}$  PRODUCTION RATE AND K-SPALLATION. *J.*  
739 *Quaternary Sci.* 29, 407–413. <https://doi.org/10.1002/jqs.2720>

- 740 Stone, J.O., 2000. Air pressure and cosmogenic isotope production. *Journal of Geophysical Research*  
741 105, 753–759.
- 742 Stone, J.O., Allan, G.L., Fifield, L.K., Cresswell, R.G., 1996. Cosmogenic chlorine-36 from calcium  
743 spallation. *Geochimica et Cosmochimica Acta* 60, 679–692. [https://doi.org/10.1016/0016-](https://doi.org/10.1016/0016-7037(95)00429-7)  
744 [7037\(95\)00429-7](https://doi.org/10.1016/0016-7037(95)00429-7)
- 745 Tomkins, M.D., Dortch, J.M., Hughes, P.D., Huck, J.J., Pallàs, R., Rodés, Á., Allard, J.L., Stimson,  
746 A.G., Bourlès, D., Rinterknecht, V., Jomelli, V., Rodríguez-Rodríguez, L., Copons, R., Barr,  
747 I.D., Darvill, C.M., Bishop, T., 2021. Moraine crest or slope: An analysis of the effects of boulder  
748 position on cosmogenic exposure age. *Earth and Planetary Science Letters* 570, 117092.  
749 <https://doi.org/10.1016/j.epsl.2021.117092>
- 750 Valadas, B., 1984. Les hautes terres du Massif central français: contribution à l'étude des  
751 morphodynamiques récentes sur versants cristallins et volcaniques. Univ. Panthéon-  
752 Sorbonne (Paris I).
- 753 Van Dorsser, H.J., 1986. La vallée du Brezon et les plateaux adjacents. *Revue de Géomorphologie*  
754 *Dynamique* 35, 113–121.
- 755 Van Dorsser, H.J., 1982. Carte géomorphologique du Sud-Ouest du Massif du Cantal. *Revue de*  
756 *Géomorphologie Dynamique* 31, 1–35.
- 757 Vergne, V., 1991. Les paysages végétaux d'Artense au Tardiglaciaire et à l'Holocène (Vegetal  
758 landscapes in the Artense region during Late-glacial and Holocene). *Bulletin de l'Association*  
759 *de Géographes Français* 68, 23–28. <https://doi.org/10.3406/bagf.1991.1555>
- 760 Veyret, Y., 1978. Les modelés et formations d'origine glaciaire dans le Massif central français :  
761 problèmes de distribution et de limites dans un milieu de moyenne montagne. Univ. Panthéon-  
762 Sorbonne (Paris I).
- 763 Veyret-Mekdjian, Y., Brousse, P., Delibrias, G., 1978. Première datation d'un épisode glaciaire récent  
764 dans le Massif central français. *Comptes rendus hebdomadaires des séances de l'Académie*  
765 *des Sciences* 286, 1089–1092
- 766 Williams, A.J., Stuart, F.M., Day, S.J., Phillips, W.M., 2005. Using pyroxene microphenocrysts to  
767 determine cosmogenic <sup>3</sup>He concentrations in old volcanic rocks: an example of landscape  
768 development in central Gran Canaria. *Quaternary Science Reviews* 24, 211–222.  
769 <https://doi.org/10.1016/j.quascirev.2004.07.004>
- 770 Wirsig, C., Zasadni, J., Christl, M., Akçar, N., Ivy-Ochs, S., 2016. Dating the onset of LGM ice surface  
771 lowering in the High Alps. *Quaternary Science Reviews* 143, 37–50.  
772 <https://doi.org/10.1016/j.quascirev.2016.05.001>
- 773 Zreda, M.G., Phillips, F.M., Elmore, D., 1994. Cosmogenic <sup>36</sup>Cl accumulation in unstable landforms:  
774 2. Simulations and measurements on eroding moraines. *Water Resources Research* 30,  
775 3127–3136. <https://doi.org/10.1029/94WR00760>

777 **9 Tables**778 **Table 1.** Characteristics of boulders for  $^{36}\text{Cl}$  surface exposure dating.

Sample ID	Latitude	Longitude	Elevation	Boulder lithology	Sample density	Shielding factor	Sample thickness
	DD	DD	(m a.s.l.)		(g.cm <sup>-3</sup> )		(cm)
<b>CTL-01</b>	44.9108	2.5019	639	basalt	3.0	1	2.0
<b>CTL-02</b>	44.9112	2.5014	646	breccia	2.6	1	3.5
<b>CTL-03</b>	44.9111	2.4984	640	breccia	2.6	1	2.6
<b>CTL-04</b>	44.9200	2.4945	818	breccia	2.6	1	1.1
<b>CTL-20</b>	44.9503	2.5897	649	breccia	2.6	0.9985	4.6
<b>CTL-21</b>	44.9509	2.5913	648	basalt	3.0	0.9985	5.9

779

780 **Table 2.** Bulk composition of samples before chemical treatment, analysed at the SARM-CRPG  
781 (Nancy, France) by ICP-OES (major elements), ICP-MS (trace element), atomic absorption (Li),  
782 colorimetry (B) and spectrophotometry (Cl). Values in italics are averages from samples CTL-02, -03  
783 for sample CTL-04.

Sample ID	SiO <sub>2</sub> %	Al <sub>2</sub> O <sub>3</sub> %	Fe <sub>2</sub> O <sub>3</sub> %	MnO %	MgO %	CaO %	Na <sub>2</sub> O %	K <sub>2</sub> O %	TiO <sub>2</sub> %	P <sub>2</sub> O <sub>5</sub> %	LOI %	Total Cl (ppm)	Li (ppm)	B (ppm)	Sm (ppm)	Gd (ppm)	Th (ppm)	U (ppm)
CTL-01	53.8	18.3	8.3	0.2	1.1	5.4	4.6	3.4	1.7	0.7	2.3	125	19.4	5.1	10.6	7.9	10.8	3.0
CTL-02	51.4	15.9	9.4	0.1	2.6	6.6	2.9	2.2	2.3	0.7	6.3	285	18.5	5.0	10.4	8.4	9.1	2.6
CTL-03	51.1	17.8	9.1	0.2	2.1	7.2	3.8	2.8	2.1	0.6	2.5	98	13.9	5.2	9.2	7.2	8.5	2.3
CTL-04	<i>51.2</i>	<i>16.9</i>	<i>9.3</i>	<i>0.1</i>	<i>2.3</i>	<i>6.9</i>	<i>3.3</i>	<i>2.5</i>	<i>2.2</i>	<i>0.6</i>	<i>4.4</i>	<i>192</i>	<i>16.2</i>	<i>5.1</i>	<i>9.8</i>	<i>7.8</i>	<i>8.8</i>	<i>2.4</i>
CTL-20	53.9	15.6	7.2	0.2	4.8	5.6	4.8	3.6	1.5	0.4	1.9	225	18.8	6.5	6.6	5.4	17.1	5.0
CTL-21	43.2	13.3	12.2	0.2	10.9	10.5	3.5	1.5	2.9	0.7	1.1	760	6.4	2.3	8.1	6.7	6.9	1.7

784

785 **Table 3.** Concentrations in major element (in %) and in Cl (in ppm) in sample splits after acid etching,  
 786 analysed at the SARM-CRPG (Nancy, France) by ICP-OES.

Sample ID	SiO <sub>2</sub> %	Al <sub>2</sub> O <sub>3</sub> %	Fe <sub>2</sub> O <sub>3</sub> %	MnO %	MgO %	CaO %	Na <sub>2</sub> O %	K <sub>2</sub> O %	TiO <sub>2</sub> %	P <sub>2</sub> O <sub>5</sub> %	LOI %	Total Cl (ppm)
CTL-01	59.39	18.69	5.27	0.06	0.63	3.79	5.25	4.14	1.72	< L.D.	0.89	99.81
CTL-02	56.75	16.41	6.03	0.09	2.83	7.65	3.41	2.63	2.27	0.16	1.47	99.69
CTL-03	55.20	15.60	9.24	0.11	2.70	6.28	3.86	3.41	2.90	< L.D.	0.45	99.75
CTL-04	58.50	16.01	6.24	0.09	2.18	6.12	3.55	3.42	2.27	0.14	1.80	100.30
CTL-20	57.13	17.78	5.02	0.08	2.60	8.75	3.20	2.18	1.43	0.15	2.15	268.53
CTL-21	56.36	19.23	4.20	0.06	1.84	7.71	3.89	2.56	1.68	0.20	1.76	98.74

787

**Table 4.** Relevant data for chemical  $^{36}\text{Cl}$  extraction, AMS results and  $^{36}\text{Cl}$  exposure ages.

Sample ID	Sample weight (g)	Mass of Cl in spike (mg)	$^{35}\text{Cl}/^{37}\text{Cl}$	$^{36}\text{Cl}/^{35}\text{Cl}$ ( $10^{-14}$ )	Number of atoms Cl ( $10^{-19}$ )	[Cl] in sample (ppm)	$^{36}\text{Cl}$ ( $10^6$ atoms)	$^{36}\text{Cl}$ ( $10^4$ at.g $^{-1}$ )	Age (ka)* including P uncertainties $\epsilon = 0$ mm yr $^{-1}$	Age (ka)* including P uncertainties $\epsilon = 10$ mm yr $^{-1}$	Age (ka)* including P uncertainties $\epsilon = 20$ mm yr $^{-1}$
<b>Plateau de Cavanhac</b>											
CTL-04**	43.59	1.8117	$3.459 \pm 0.059$	$11.1 \pm 0.8$	$38.60 \pm 7.03$	$521 \pm 95$	$35.80 \pm 6.42$	$82.14 \pm 14.73$	$16.9 \pm 3.9$ (4.9)	$13.5 \pm 3.9$ (4.9)	$13.3 \pm 3.9$ (4.9)
<b>Moraine de Carnéjac</b>											
CTL-01	42.97	1.8020	$8.703 \pm 0.150$	$14.8 \pm 0.9$	$2.25 \pm 0.13$	$31 \pm 2$	$7.07 \pm 0.48$	$16.44 \pm 1.11$	$12.0 \pm 1.2$ (1.3)	$12.6 \pm 1.2$ (1.3)	$13.9 \pm 1.2$ (1.3)
CTL-02**	44.09	1.8020	$3.757 \pm 0.067$	$9.5 \pm 0.7$	$20.20 \pm 2.34$	$270 \pm 31$	$17.38 \pm 2.10$	$39.42 \pm 4.76$	$13.6 \pm 2.2$ (3.0)	$12.0 \pm 2.2$ (3.0)	$12.1 \pm 2.2$ (3.0)
CTL-03	40.41	1.8096	$8.684 \pm 0.262$	$13.7 \pm 0.8$	$2.27 \pm 0.16$	$33 \pm 2$	$6.57 \pm 0.44$	$16.26 \pm 1.09$	$11.8 \pm 1.1$ (1.3)	$12.2 \pm 1.1$ (1.3)	$13.2 \pm 1.1$ (1.3)
<b>Moraine de Polminhac</b>											
CTL-20	45.07	2.0010	$3.807 \pm 0.115$	$8.9 \pm 0.5$	$20.56 \pm 3.60$	$269 \pm 47$	$17.01 \pm 2.65$	$3.78 \pm 0.59$	$13.6 \pm 2.6$ (2.6)	$12.1 \pm 2.6$ (2.6)	$12.3 \pm 2.6$ (2.6)
CTL-21**	45.15	1.9998	$4.961 \pm 0.149$	$1.8 \pm 0.2$	$7.57 \pm 0.72$	$99 \pm 9$	$1.64 \pm 0.18$	$0.36 \pm 0.04$	$0.96 \pm 0.3$ (0.3)	$0.9 \pm 0.3$ (0.3)	$0.9 \pm 0.3$ (0.3)
BKCTL-01	-	1.7632	$376.034 \pm 9.772$	$0.23 \pm 0.06$	-	-	-	-	-	-	-
BKCTL-02	-	1.9914	$212.416 \pm 8.504$	$0.012 \pm 0.004$	-	-	-	-	-	-	-

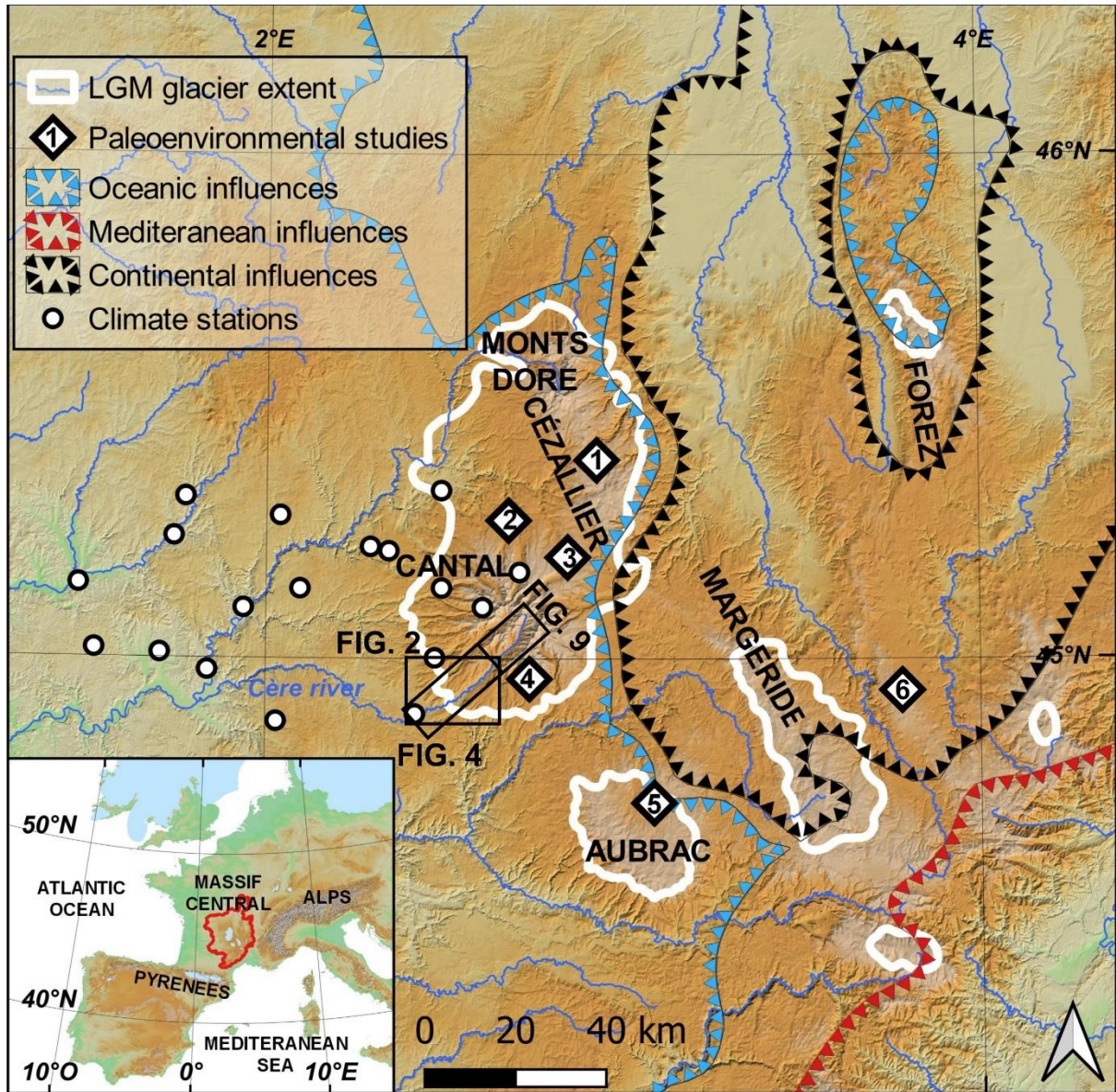
\* No snow correction.  
\*\* Cl- rich sample

790 **Table 5.** Synthesis of Carnéjac and Polminhac Equilibrium Line Altitude (ELA) reconstructions and  
 791 associated climatic conditions using local Mean July Temperature (MJT) for the Younger Dryas and  
 792 the Oldest Dryas.

	ELA (m)	Current climatic conditions at ELA altitude		Roustières site (1196 m a.s.l.)			
		MST (°C)	MAP (mm.yr <sup>-1</sup> )	Younger Dryas climatic conditions at ELA		Oldest Dryas climatic conditions at ELA	
				MST (°C)	MAP anomaly (%)	MST (°C)	MAP anomaly (%)
Carnéjac stade (post-RSF topography)	1091 ± 43	15.5 ± 0.2	1771 ± 36				
Carnéjac stade (pre-RSF topography)	1078 ± 43	15.5 ± 0.2	1760 ± 37	9.5 - 12.4	+230 - +305	5.7 - 9.5	+141 -+230
Polminhac stade	1152 ± 34	15.2 ± 0.2	1823 ± 29				
Today	2759 ± 28	7 ± 1	3162 ± 159	-	-	-	-

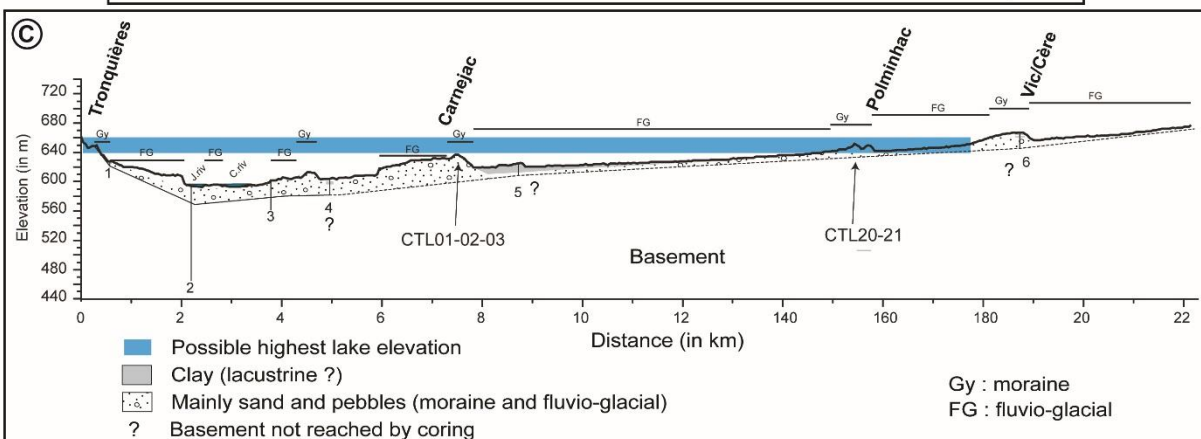
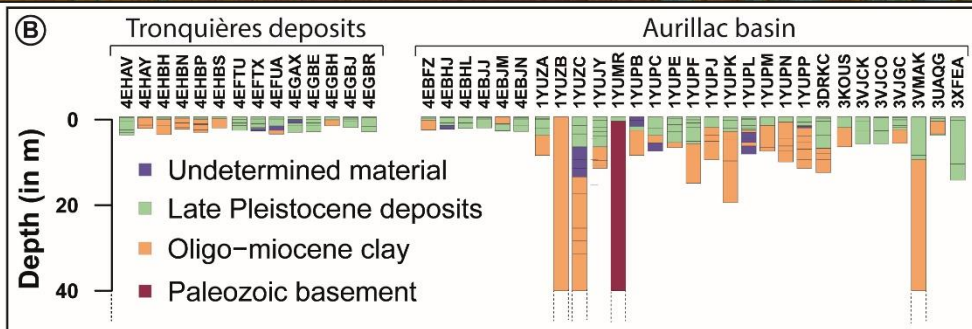
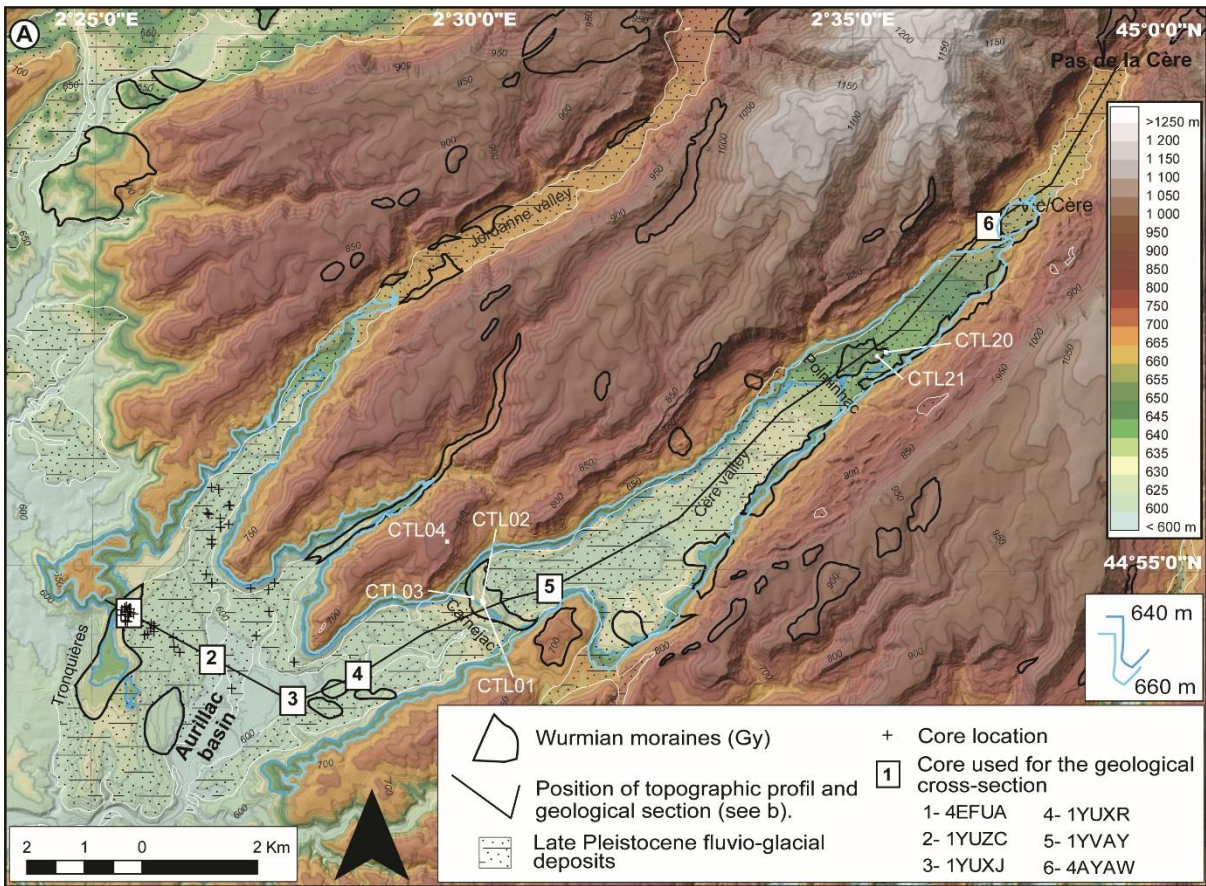
793





795

796 **Figure 1.** Location map of the Cère Valley in the Cantal-Cézallier-Mont Dore glacial system (CCMD),  
 797 with Local Last Glacial Maximum (LLGM) extent in the Massif Central (Ehlers et al., 2011), and main  
 798 actual atmospheric influences. Numbers correspond to localities cited in the main text: 1) Godivelle, 2)  
 799 Lugarde kame terrace from where the  $^{14}\text{C}$  age was obtained, 3) Taphanel, 4) Peyre, 5) Roustières, 6)  
 800 Lake Bouchet.



801

802 **Figure 2.** A. Map of glacial and associated deposits in the lower Cère Valley, between the Pas de la  
 803 Cère and the Aurillac basin, according to the 1:50000 geological survey map (Brousse et al. 1972)  
 804 and location of geological cores (data available at <http://infoterre.brgm.fr>). B. Interpretation of  
 805 geological cores from the Tronquières moraine and the Aurillac basin. C. Interpreted geological cross-

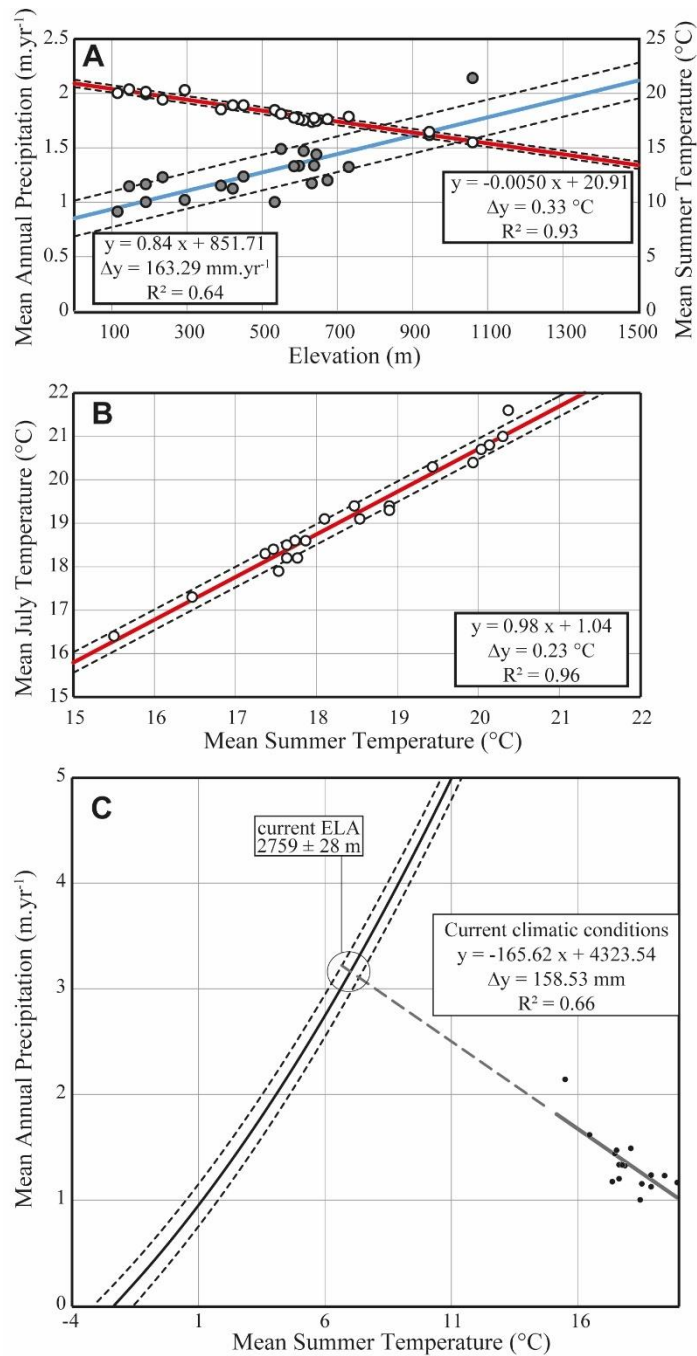
806 section of the lower Cère valley, using geological survey map (1:50000) and most develop geological  
807 cores.



808

809 **Figure 3.** Photographs of erratic boulders sampled for  $^{36}\text{Cl}$  surface exposure dating. Fractures of CTL-  
 810 01 boulder are highlighted with white dashed lines.

811



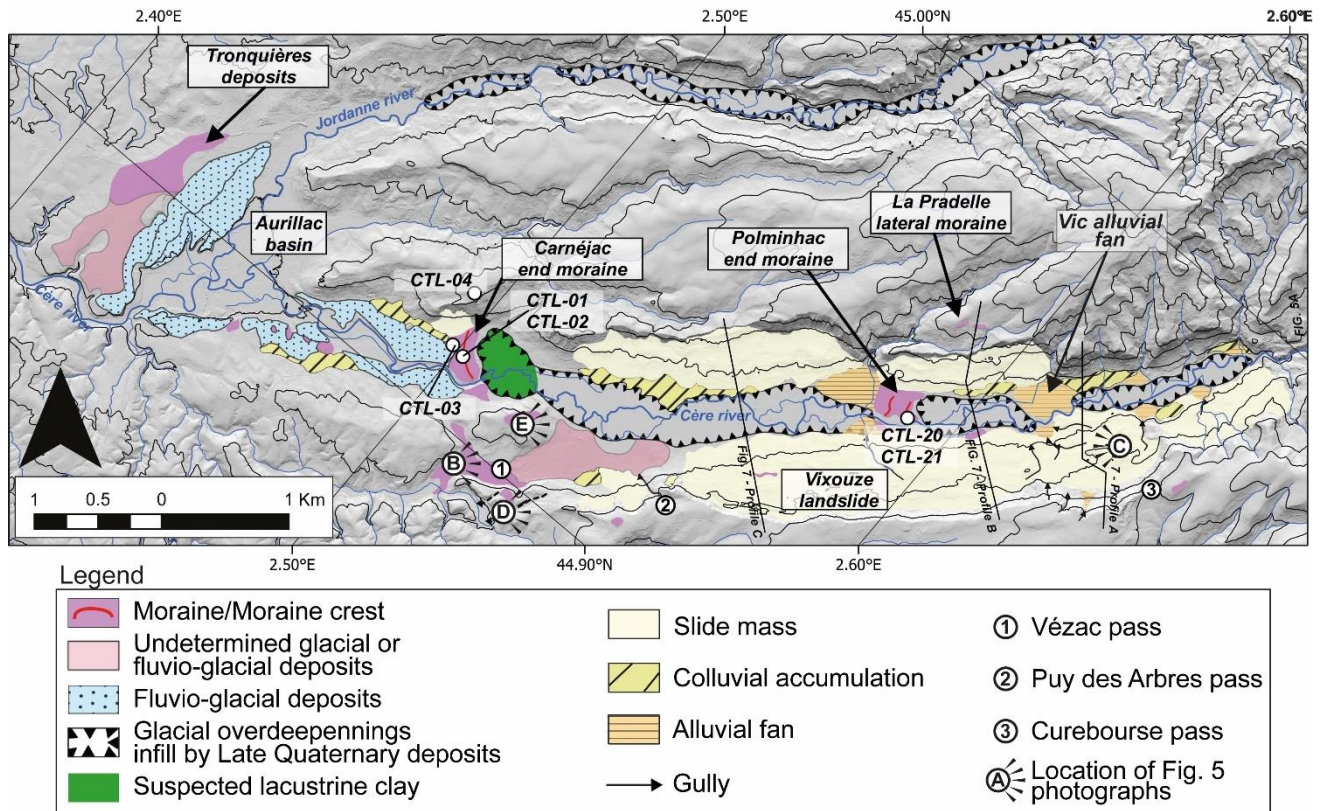
812

813 **Figure 4.** Climatic conditions in the western Cantal. A) Mean Summer Temperature (MST) and  
 814 Mean Annual Precipitation (MAP) from the 21 climatic stations, plotted against elevation and  
 815 associated elevation gradients. Black dots are mean annual precipitation. White dots are mean  
 816 annual temperatures. B) Linear regression of Mean July Temperature (MJT) against Mean Summer  
 817 Temperature (MST). C) Calculated current theoretical ELA from interpolation of the 21 climatic  
 818 stations against the Ohmura equation.



819

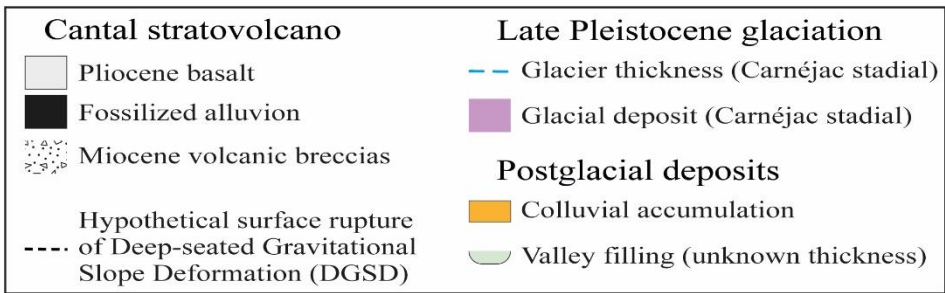
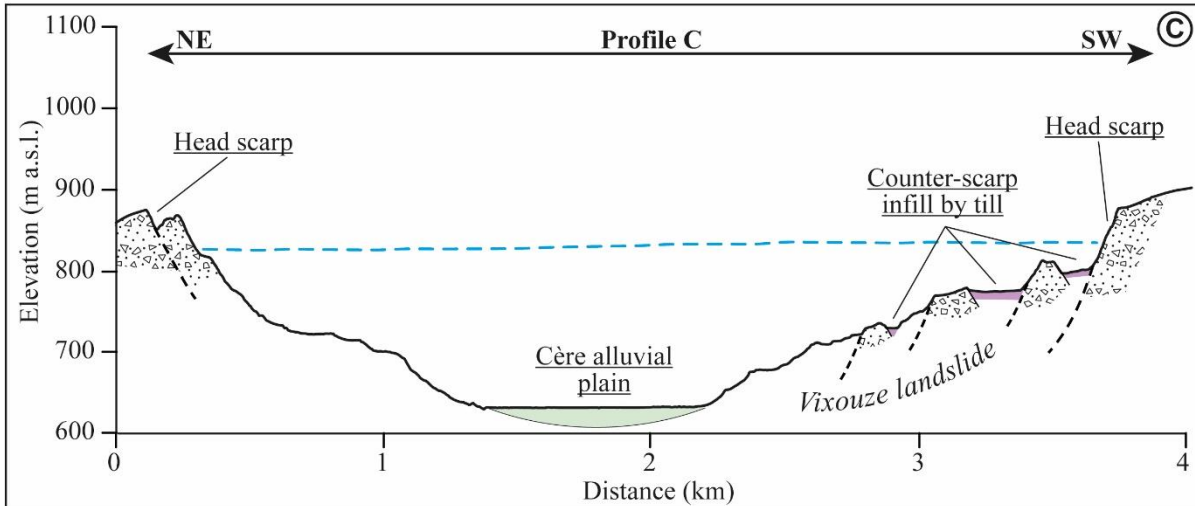
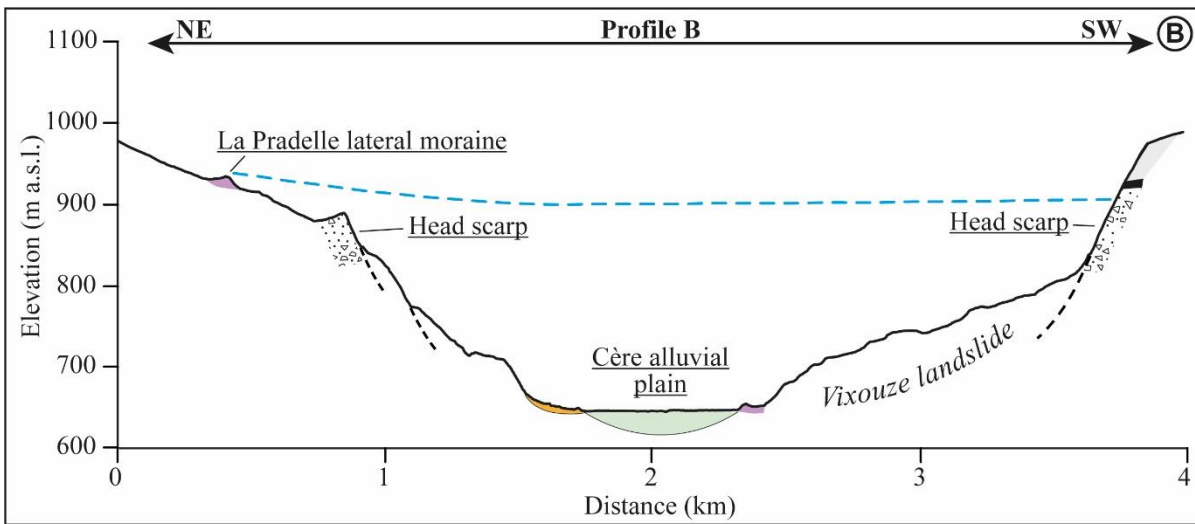
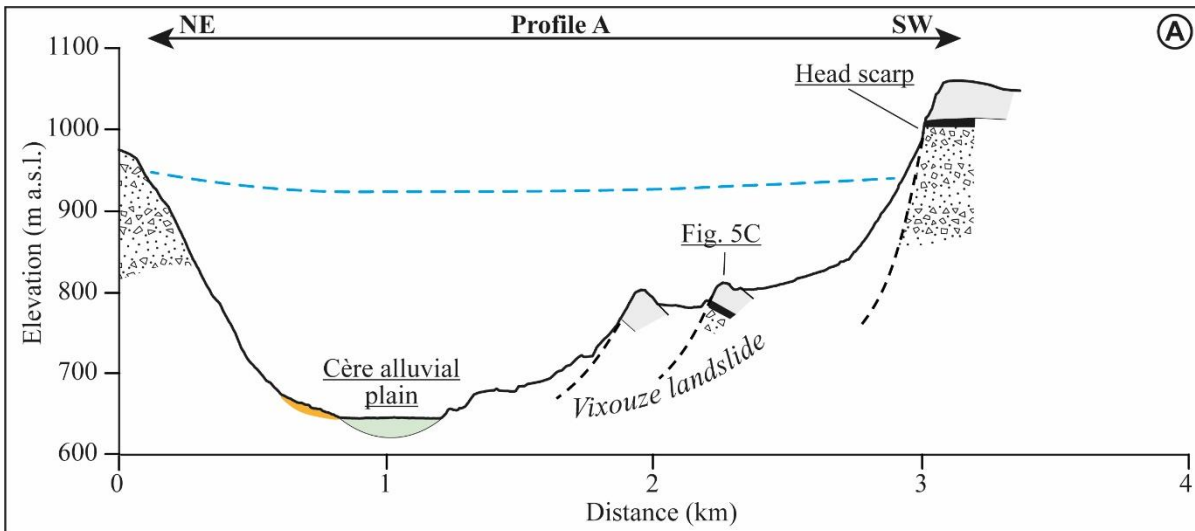
820 **Figure 5.** Photographs of geomorphological features in the Cère Valley. A) The Fond d'Alagnon glacial  
 821 cirque and the Alagnon glacier transfluence towards the Cère Valley. B) Basal till deposits (LLGM) at  
 822 the Vézac pass. C) Fossilized alluvion under basaltic table in the Vixouze landslide constituting slide  
 823 masses. D) Ice-marginal deposits (LLGM) forming terraces at the Vézac pass. E) View of the lower  
 824 Cère Valley, showing the extent of the Vixouze landslide.



825

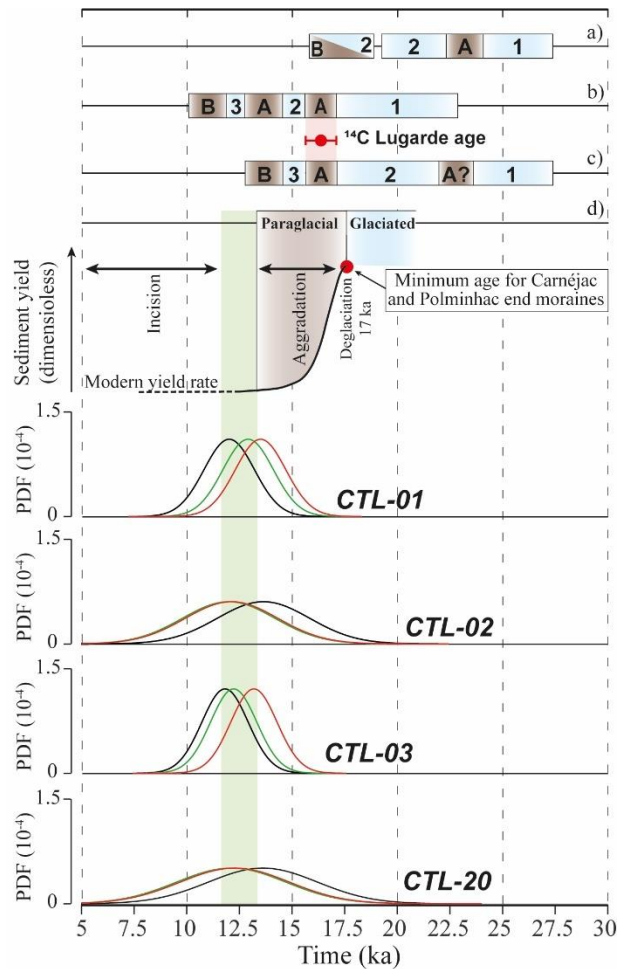
826 **Figure 6.** Map of glacial and slope deposits and location of the  $^{36}\text{Cl}$  samples in the lower part of the

827 Cère Valley.



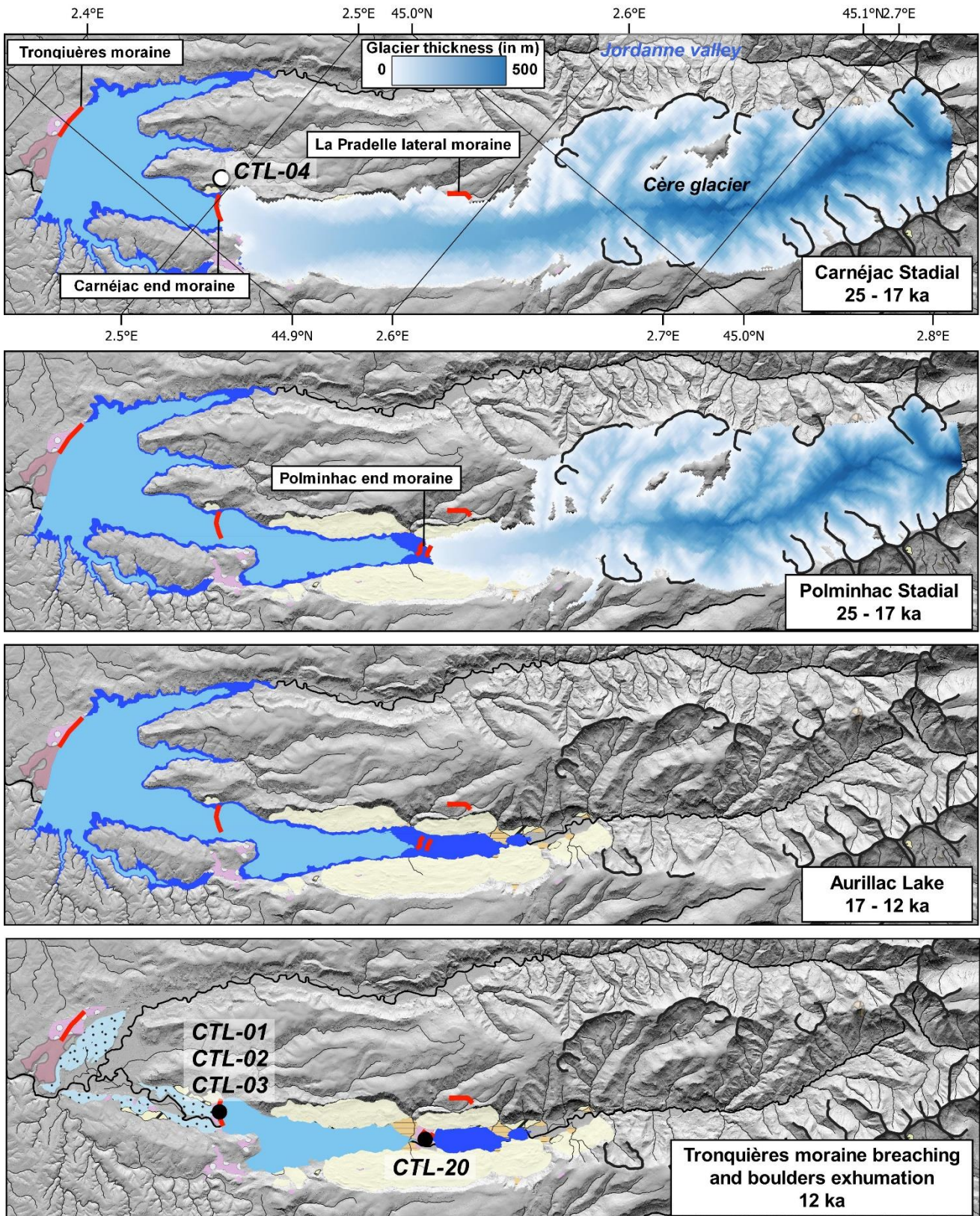


829 **Figure 7.** Transverse profiles of the lower Cère Valley showing relationships between Deep-seated  
830 Gravitational Slope Deformations (DGSDs) and the former glacier. A. Transversal profile located  
831 upstream the Vic alluvial fan. B. Transversal profile located upstream the Polminhac end moraine. C.  
832 Transversal profile located upstream the Carnéjac end moraine. For precise location of profiles see  
833 Figure 6.



834

835 **Figure 8.** Camel plots of  $^{36}\text{Cl}$  exposure ages under different erosion rate scenarios (black line:  $0 \text{ mm.ka}^{-1}$ ,  
836  $1$ , green line:  $10 \text{ mm. ka}^{-1}$ , red line:  $20 \text{ mm. ka}^{-1}$ ) against local glacial chronologies and the chronological  
837 scenario of postglacial evolution of the Cère Valley. Camel plots were generated using the Matlab code  
838 from G. Balco (<https://cosmognosis.wordpress.com/2009/07/13/matlab-code-for-camel-diagrams/>). a)  
839 Glacial chronology of the Aubrac plateau icefield from  $^{10}\text{Be}$  and  $^{26}\text{Al}$  exposure ages (Ancrenaz et al.,  
840 2022). b) Relative glacial chronology established by Veyret (1978) for the CCMD last glaciation. c)  
841 Relative glacial chronology established by Etlicher and Göer de Hervé (1988) for the CCMD last  
842 glaciation. 1: Local Last Glacial Maximum, 2: Minor glacier advance, 3: Cirque glacier stade, A: Glacier  
843 retreat, B: Full deglaciation. d) Schematic representation of the sediment yield during the paraglacial  
844 period (modified from Ballantyne, 2002) against our chronological scenario for the deglaciation, the  
845 postglacial and the ‘modern’ periods. The convergence of  $^{36}\text{Cl}$  exposure ages (green box) is interpreted  
846 as the end of the paraglacial period and the beginning of the ‘modern’ period (see text for more details).



847

848 **Figure 9.** Reconstruction of the last deglaciation in the Cère Valley according to the Aurillac proglacial  
 849 Lake scenario. Two lake levels were represented: 640 m in light blue and 660 m in dark blue. Black  
 850 lines delineated glacial cirques. For the legend see Fig. 6.